Carbon dynamics driven by seawater recirculation and groundwater discharge along a forest-dune-beach continuum of a high-energy meso-macro-tidal sandy coast

Céline Charbonnier, Pierre Anschutz, Gwenaël Abril, Alfonso Mucci, Loris Deirmendjian, Dominique Poirier, Stéphane Bujan, Pascal Lecroart

Carbon dynamics driven by seawater recirculation and groundwater discharge along a forest-dune-beach continuum of a high-energy meso-macro-tidal sandy coast

Céline CHARBONNIER[1], Pierre ANSCHUTZ[1,*], Gwenaël ABRIL[1,2,3], Alfonso MUCCI[4], Loris DEIRMENDJIAN[1,§], Dominique POIRIER[1], Stéphane BUJAN[1], and Pascal LECROART[1]

1 Univ. Bordeaux, CNRS, EPOC, EPHE, UMR 5805, F-33600 Pessac, France

2 Biologie des Organismes et Ecosystèmes Aquatiques (BOREA), Muséum National d'Histoire Naturelle, FRE 2030, CNRS, MNHN, IRD, SU, UCN, UA, Paris, France

3 Programa de Geoquímica, Universidade Federal Fluminense, Niterói, RJ, Brazil

4 GEOTOP and Department of Earth and Planetary Sciences, McGill University, Montreal QC, Canada

§ Present address: Université Paul Sabatier-IRD-OMP-CNRS, UMR Geosciences Environnement Toulouse, France

* Corresponding author : pierre.anschutz@u-bordeaux.fr

Abstract

High-energy tidal beaches are exposed to strong physical forcings. The submarine groundwater discharge (SGD) that occurs in intertidal sandy sediments includes both terrestrial, fresh groundwater flow and seawater recirculation, and plays a significant role in regulating biogeochemical cycles in some coastal zones. In this transition zone between land and sea, complex biogeochemical reactions alter the chemical composition of pore waters that discharge to the coastal ocean. Recent studies highlight that SGD can be a significant source of carbon to the coastal ocean but very few have investigated SGD in high-energy environments. We have characterized the dissolved carbon dynamics in such a high-energy environment (Truc Vert Beach, SW France) through pore water sampling in key compartments of the SGD system. Dissolved organic carbon (DOC), pH, total alkalinity (TA), and the isotopic composition of dissolved inorganic carbon (δ^{13}C-DIC) were measured in pore waters sampled at regular intervals between 2011 and 2014 in the intertidal zone of the beach, the mixing zone of the subterranean estuary (STE), and the freshwater aquifer upstream from the beach. Results reveal that SGD exports dissolved carbon mostly as DIC to the Aquitaine coast some of which originates from the aerobic respiration of marine organic matter within the beach aquifer. This is highlighted by the opposite spatial trend of DOC, which is consumed, and DIC, which is produced. Saline pore waters expelled from the beach through tidally-driven recirculation of seawater provide about 4400 tons of carbon per year to the coastal zone of the 240 km-long Aquitaine sandy coast. Terrestrial groundwater, characterized by high pCO_2 values, is also a significant contributor to the DIC flux to the coastal ocean (16200 tons per year). This flux is abated by CO_2 evasion in the upper beach, at the onset of the salinity gradient in the STE, and within the surficial freshwater aquifer along the forest-beach transect below the coastal foredune. Accordingly, the DIC:TA ratio evolves to below 1, suggesting that this SGD increases the buffer capacity of coastal seawater against acidification. This study demonstrates that high-energy beaches are active vectors of DIC from the land to the coastal ocean as well as significant sources of CO_2 to the atmosphere, and must therefore be taken into consideration in SGD carbon budgets.

Keywords: tidal beach; submarine groundwater discharge; subterranean estuary; aerobic benthic respiration; CO2 degassing; Aquitaine coast

1. Introduction

A better understanding of the carbon cycle in coastal zones is critical as these environments are especially vulnerable to global warming and ocean acidification (Gattuso et al., 1998; Orr et al., 2005; Gattuso and Hansson, 2011). Groundwater discharge through permeable coastal sediments is now recognized as an important phenomenon, connecting continental aquifers to the coastal ocean through subterranean estuaries (STE) (Moore, 1999; Bokuniewicz et al. 2003; Burnett et al., 2003; Santos et al., 2012a). The behaviour of dissolved carbon in this transition zone needs to be studied in different physical settings (topography, flow, tides) in order to better constrain the role of submarine groundwater discharge (SGD) on the global, coastal carbon cycle. In intertidal sandy sediment, SGD includes both freshwater flow from a terrestrial aquifer and seawater recirculation driven by waves and tides (Burnett et al., 2003). In high-energy sandy beaches, a well-developed intertidal seawater recirculation cell develops as a result of strong physical forcings, including tidal oscillations, swells, waves, and beach topography (Robinson et al., 2007; Abarca et al., 2013). This cell complements the structure of the subterranean estuary (STE) formed between fresh and saline groundwaters (Moore, 1999).

The influence of SGD fluxes on coastal ecosystems is well documented for nutrients and trace metals, with fluxes (Burnett et al., 2003; 2006; Slomp and Van Cappellen, 2004; Kim et al., 2005). This can lead to pronounced ecological consequences in the coastal zone, such as eutrophication (Lee and Kim, 2007; Lee et al., 2010; Moore et al., 2010; Wang et al., 2018) and harmful algal blooms (Lee et al., 2010), especially in semi-enclosed systems (Liu et al., 2012; Charette et al., 2013; Santos et al., 2014). Over the last decade, the carbon cycle in STEs has received growing attention, because STEs are sites of intense biogeochemical transformations. As observed for nutrients, trace metals and/or radio-isotopic tracers (Slomp and Van Cappellen, 2004; Charette et al., 2005; Moore, 2006; Swarzenski et al., 2006), the transfer of carbon from land to the sea is not conservative: significant chemical transformations linked to diagenetic reactions in the STE affect the CO_2 system through carbonate dissolution and/or organic matter mineralization (Cai et al., 2003; Liu et al., 2012; Lee and Kim, 2015; Liu et al., 2017). Although the relative importance of all carbon transfer processes from land to sea are not always considered, recent studies reveal that the terrestrial component of SGD is a significant carbon source to the coastal ocean (Liu et al., 2012; Atkins et al., 2013; Wang et al., 2015; Liu et al., 2017). Indeed, fresh groundwaters are often enriched in CO_2 due to organic matter mineralization within the surficial aquifer (Gagan et al., 2002; Savoy et al., 2011). They are

93 also enriched in dissolved organic carbon (DOC), although marine-derived particulate matter
94 may be the primary source of DOC in tidal sands (Couturier et al., 2017). These waters can
95 modify the carbon budget as they discharge in the coastal zone (Cai et al., 2003; Moore et al.,
96 2006; Liu et al., 2012; Santos et al., 2012b). In fact, a number of studies have reported that
97 terrestrial groundwater discharge can be a significant source of CO_2 and CH_4 to the atmosphere
98 in coastal areas (Cai et al., 2011; Atkins et al., 2013; Call et al., 2015; Perkins et al., 2015).
99 Dissolved carbon fluxes from SGD have been investigated in various environments
100 including estuaries (Santos et al., 2012a; Faber et al., 2014; Macklin et al., 2014; Sadat-Noori
101 et al., 2015; Wang et al., 2015), a coral reef lagoon (Cyronak et al., 2013), mangrove creeks
102 (Bouillon et al., 2007; Koné and Borges, 2008; Miyajima et al., 2009; Maher et al., 2013; Call
103 et al., 2015; Chen et al., 2018), continental shelves (Liu et al., 2012, 2014; Stewart et al., 2015),
104 and intertidal flats (Moore et al., 2011; Kim et al., 2012; Reckhardt et al., 2015; Santos et al.,
105 2015), but very few studies have been carried out in high-energy beaches, even if the intertidal
106 recirculation cell in such environments has been recognized as an intense biogeochemical
107 reactor (Anschutz et al., 2009; Charbonnier et al., 2013; Beck et al., 2017; Reckhardt et al.,
108 2015). Recent studies show that recirculated saline pore water can deliver large amounts of
109 recycled inorganic carbon to coastal surface waters (Weinstein et al., 2007; Gleeson et al., 2013;
110 Liu et al., 2014).
111 The objective of this study was to identify biotic and abiotic processes that
112 modulate/drive carbon dynamics in a very high-energy coastal system. These environments are
113 characterized by a very strong recirculation of seawater due to tidal pumping. Since the fresh
114 and saline SGD components are usually superimposed, it is difficult to separate their relative
115 contributions. We first investigated whether the large volumes of water exchanged in the sandy
116 beach aquifer resulted in a high carbon recycling. We then evaluated the carbon fluxes from the
117 terrestrially-derived groundwater that percolated towards the beach. In doing so, we tested the
118 hypothesis that, like metals and nutrients, DIC fluxes are not conservative when water from the
119 continental aquifer mixed with saline water from the intertidal beach aquifer. Fluxes and
120 processes were assessed from samples collected along the forest-dune-beach continuum.
121 Finally, we estimated, for the first time, carbon fluxes to the ocean and atmosphere at the scale
122 of a 240-km long exposed coastline, allowing us to assess the importance of these systems in
123 the carbon cycle and their impact on ocean acidification.
124 For this purpose, we deployed an elaborate sampling strategy, from land to sea, which
125 allowed us to measure DOC, pH, total alkalinity (TA), and the isotopic composition of
126 dissolved inorganic carbon (δ^{13}C-DIC), as well as calculate the dissolved inorganic carbon

(DIC) and CO_2 partial pressure (pCO_2) in pore waters of all key compartments of a high-energy sandy beach along the Aquitaine coast (SW France) over multiple years. Pore water samples were collected in the intertidal beach, in the fresh-saline transition zone of the supratidal beach, and in the freshwater aquifer upstream of the beach

2. Materials and methods

2.1. Study site

The Truc Vert Beach is located a few kilometres north of the Cap Ferret sand spit, along the 240-km long Aquitaine sandy coast (SW France; Fig. 1). The beaches along this relatively straight coastline, between the Gironde and the Adour Estuaries, are meso-macro tidal and double-bar beaches subjected to high-energy conditions and bordered by high aeolian dunes (Castelle et al., 2007). The Truc Vert Beach is typical of the Aquitaine coast and its difficult access has preserved it from human disturbance.

Sediment consists of medium-sized quartz sand with a mean grain size of 435 μm, a mean $CaCO_3$ content of 1.2 wt% and a mean organic carbon concentration of 0.028 wt%. The porosity of the sand ranges from 0.38 to 0.42 (Charbonnier et al., 2013). The average tidal range is 3.2 m, extending up to 5 m during spring tides. The high tide water line is marked by the presence of scattered debris that consist mainly of driftwood, shells, minor plastic waste, and marine plants. The mean wave amplitude is 1.5 m, but can reach up to 10 m during winter storms. Ridge and runnel systems develop depending on meteorological conditions (Michel and Howa, 1999; Castelle et al., 2007).

The tidal regime, swells, and meteorological conditions influence the cross-shore topography of the beach and can generate large sand movements, with observed sand accretion or erosion exceeding 1 m within a few days at any given location (Castelle et al., 2014). The extension of the intertidal zone also varies depending on topography, tidal range, and wave regime, with a beach width ranging from 80 to 200 m cross-shore. At high tide, the beach is immersed and the sand is saturated with water. At low tide, the sand surface of the lower beach remains saturated with water, whereas the water table (i.e., the boundary between the unsaturated and saturated zones of the sediment) at the upper beach stands more than one meter below the sand surface. Pore waters seeping out at the lower beach indicate that a large volume of water is flushed seaward at each ebbing and low tide. The seepage zone is located along a 10-50 m wide cross-shore region of the lower beach. The volume of pristine seawater entering

161 the sand during each rising tide was estimated at approximately 15 m^3 per longshore meter
162 (Charbonnier et al., 2013; Fig. 2). Integrated over the whole Aquitaine coastline, the volume of
163 seawater recirculating through the beach aquifer is about 2.5 km^3 each year.
164 The beach catchment, i.e., the land area that is directly drained by the beach (no drainage
165 through rivers or lakes), was contoured using the Geographic Information System (GIS)
166 ArcGIS. It is a 0 to 10 km wide strip of wooded land along the 240-km long coastline and
167 covers 822 km^2 (Anschutz et al., 2016). This coastal aquifer is composed of sand dunes, marine
168 sands, and gravels of the Plio-Quaternary period. It is very permeable (Legigan, 1979) and
169 sustains a terrestrial groundwater flux from the continent to the ocean through the percolation
170 of brackish waters through the beach (Charbonnier et al., 2013; Anschutz et al., 2016). The
171 volume of these discharging fresh groundwaters, estimated from a water balance calculation of
172 the precipitation (about 810 mm y^{-1} at the Truc Vert Beach) and evapotranspiration (max. 570
173 mm y^{-1}), is approximately 0.2 km^3 per year for the whole Aquitaine coast (Fig.2; Anschutz et
174 al., 2016). A revised value that takes into account the distribution of mean precipitations from
175 the northern to the southern part of the coast, and not solely the value of the Truc Vert Beach,
176 yields a value of 0.43 km^3 yr^{-1} (Anschutz et al., 2017).
177
178 2.2. Sampling
179
180 A variety of waters were sampled, including seawater, intertidal and supratidal beach
181 pore waters, waters from the unconfined surficial aquifer located at the foot of the dune, and
182 terrestrial groundwaters (Fig. 2). This assorted sample collection allowed us to construct a
183 complete profile of the drainage waters from the forest watershed to the intertidal zone of the
184 beach. In all cases, temperature, salinity, dissolved oxygen saturation, and pH were recorded
185 on-site within 1 min of pore water retrieval using WTW probes. The probes were calibrated
186 before and after each field campaign using an oxygen-free solution and an aerated solution
187 (100% saturation) for the oxygen saturation, with IAPSO standard seawater and deionized
188 water for the salinity, and with NIST-traceable buffer solutions (pH =4.01 and pH = 7.00 at
189 25°C) for the pH. Oxygen and salinity probe readings were compensated automatically for in-
190 situ temperature. When appropriate, the influence of salinity on the oxygen saturation was
191 recalculated.
192 Waters destined for DOC analysis were sampled with a clean 50-mL glass syringe,
193 filtered through pre-combusted (550°C) GF/F filters (porosity of 0.7 μm) into detergent-washed
194 and pre-combusted Pyrex vials (30 mL), acidified with 50 μL of a 37% HCl solution to pH 2,

and stored at 4°C. Waters for TA measurements were sampled using a 50-mL plastic syringe, filtered through a 0.45 μm cellulose acetate syringe-membrane into 150 mL polypropylene bottles. To analyse δ^{13}C-DIC, we sampled waters with a homemade funnel with a hose attached at the nozzle and from which we overfilled 100 mL glass serum vials. Glass bottles were sealed and samples were poisoned with 0.3 mL of a saturated $HgCl_2$ solution to avoid bacterial activity. Samples were stored in the dark before analysis.

2.2.1. Seawater and intertidal beach pore waters

Seawater and pore waters of the intertidal zone were sampled every two weeks during the spring tide periods and primarily on non-rainy days from February 2011 to November 2012. Pore water sampling was conducted at low tide by digging holes along cross-shore transects to reach the top of the water table. The use of permanently installed piezometric wells to collect pore waters was ruled out because of the high-energy conditions in the intertidal zone. In previous attempts, piezometers were broken or quickly buried in the sand, sometimes after a single tidal cycle. Thirty-seven profiles were obtained during the 22 months of monitoring. Parallel cross-shore transects were also carried out three times in 2012 for nutrient analyses and revealed that longshore spatial patchiness was low (Charbonnier et al., 2013).

Holes were dug every 10 m from the low-tide water line to the high- tide watermark (Fig. 2). They were deep enough to reach the top of the water-saturated zone in the sand: one shovelful was needed in the lower beach, whereas more than 1.5 m deep holes were required in the upper beach. Whereas this method is invasive, given time and physical constraints, it is the only one that allowed us to obtain representative samples. Other sampling protocols, such as the use of piezometer wells and push-point pore-water samplers (lance), were tried, but were not practical or had major drawbacks. Because of shifting sand during storms, piezometers were often exposed, broken by waves and filled with sand, even above the high spring tide water line At deep sites on the upper beach, the insertion, pore water extrusion, and extraction of a lance could not be completed before the next rising tide. Furthermore, as we did not have prior knowledge of the depth of the water table, we still had to dig a hole to determine this variable. The depth of the water table in the holes was between 10 and 15 cm. To insure the integrity of the pore water recovered at the bottom of the holes, water that initially filled the bottom of the hole, once we reached the water table, was scooped up with a polypropylene beaker. Given the high permeability of the sand, the hole was refilled with new interstitial water within a few seconds and this water was sampled with the beaker. Hence, we believe that the water was

freshly extracted from the interstitial medium. An oxygen sensor was placed immediately at the bottom of the renewed puddle and allowed to equilibrate for a few minutes. . Once it stabilized, the probe reading (O_2 saturation) remained nearly invariant, even if the water was strongly depleted in dissolved O_2. In the summer of 2011, we observed anoxic waters (0% O_2 saturation) in several lower beach holes, implying that during the measurement, there was neither significant O_2 contamination and nor gas exchange with the atmosphere. The digging operation, in-situ measurements and samplings took from 5 to 20 min per hole.

At selected periods during this study, autonomous Aanderaa optodes and NKE data loggers were buried directly into the sediment and the in-situ oxygen saturations at the water table at low tide over several tidal cycles (Charbonnier et al., 2016). Among these deployments, two vertical profiles composed of three probes separated from each other by 10 to 20 cm were carried out. These probes recorded O_2 saturations around 60% at the time of the deployments. These results were identical along the full profile, particularly at low tide, the period corresponding to our sampling in the dug holes. Results of the autonomous measurements were always close to those measured directly in holes with the WTW O_2 sensor, implying that on the scale of the thickness of the water table sampled from holes (about 10 cm), the water mass is homogeneous and that our sampling strategy was appropriate for this type of highly permeable medium.

2.2.2. Supratidal wells

In February 2013, three 7 m-long piezometers were deployed at supratidal sites upstream of the intertidal zone of the Truc Vert Beach, between the high tide mark and the dune foot (Fig. 2). Measurements and samplings were carried out every day during one full lunar cycle in February and March 2013 as well as in September and October 2013. The dates were chosen according to the elevation of the terrestrial water table, which is generally shallowest at the end of winter and deepest in October.

In each piezometer, three 5-mm inner diameter Tygon tubes were firmly fixed at three different depths (from 1.5 to 6 m depth) in order to construct a vertical profile. Samples were collected at low tide by pumping with a 60-mL syringe, after flushing several void volumes to rinse the tubes. We did not purge the whole well volume because of the high permeability of the beach sand and to avoid mixing.

At low tide, the upper part of the three piezometers was filled with air because the water table was deeper. It was likewise the case at high tide for the upper piezometer (i.e., closest to

263 the dune foot). Thus, it was not always possible to recover waters from all Tygon tubes and, in
264 most cases, waters were only collected from the deepest one. Waters recovered at three different
265 depths within a given piezometer were identical in composition, implying that the supratidal
266 aquifer was homogeneous over the sampled depths.
267 Since the piezometers were made of plastic (PVC) and we used Tygon tubing, we
268 suspected that the DOC samples were contaminated and, thus, were discarded . Due to the high
269 volume (100 mL) of water required for δ^{13}C-DIC analyses, these samplings were performed
270 only twice during the February-March 2013 campaign, once during the spring tide and once
271 during the neap tide. In addition to the WTW probe measurements, oxygen concentrations and
272 temperatures were also recorded with Aanderaa 3835 optodes equipped with NKE data loggers
273 located at each sampling point of the three piezometers. These probes had a precision of ± 5 %
274 for oxygen and ± 0.1°C for temperature and were tested in the laboratory before and after each
275 field deployment. As observed from the water sampling, probe data were identical at the
276 different depths within the same piezometer, further supporting the hypothesis of a
277 homogeneous surficial aquifer at the beach face.
278 The water table level in the piezometers was also monitored continuously with
279 CeraDIVER sensors (Schlumberger®). These probes measured water pressure and converted it
280 into a hydraulic head with a precision of ± 0.2 cm. In addition, atmospheric pressure at the study
281 site was recorded with a BaroDIVER (Schlumberger®) placed at the top of the dune. Hydraulic
282 head data were corrected for atmospheric pressure variations and referenced to zero sea level
283 using the DiverOffice software (Schlumberger®).
284
285 2.2.3. Terrestrial groundwater
286
287 We sampled terrestrial groundwater, directly drained by the beach, from wells located
288 behind the sand dune in the pine forest (Fig. 2). Built to fight forest fires, these wells are about
289 10 m deep and are always drilled within the freshwater aquifer. Depending on the position of
290 these wells on the dunes, the piezometric height was between 0.5 and 6 m deep, whereas the
291 annual vertical oscillation of the water height is about 1.5 m (Buquet, 2017). Waters were
292 sampled 2 m below the water table using two centrifugal submersible pumps (Xylem LVM
293 105) connected in line to a 1/2" nylon tubing. Water was left to overflow a beaker in which
294 WTW probes continuously measured conductivity, temperature, pH, and dissolved oxygen.
295 Once the probe readings had stabilized, samples were withdrawn for chemical analyses.
296 Depending their ease of access, some wells were sampled three times in 2013-2014, whereas

some others were sampled only once. These wells are made of PVC and we used nylon tubing to pump the water up, but since we were able to purge the system several times by pumping more than 100 L before sampling, we deemed that the collected water was not contaminated for DOC measurements.

2.3. Analyses

DOC concentrations were determined by the high temperature catalytic oxidation method using a Shimadzu TOC 5000 analyser after removing DIC by bubbling oxygen through the acidified samples (Sharp, 1993). The instrument was calibrated using a standard potassium phthalate solution of, diluted to different concentrations according to the estimated DOC content of the samples. The precision of these measurements was about 10 μM, based on replicate analyses of the same samples. TA was measured on 50 mL filtered samples by automated potentiometric titration (Metrohm 794 Basic Titrino®), with a combined pH glass electrode (Metrohm 6.0262.100®) and 0.1N HCl solution as a titrant. The equivalence point of the titration was determined by the Gran linearization method (Gran, 1952). Replicates were performed (two per sampling station) and precision was about 2 μM. From these TA measurements and the in-situ pH, salinity, and temperature, we calculated DIC concentrations and pCO_2 values using the carbonic acid dissociation constants of Mehrbach et al. (1973) refitted by Dickson and Millero (1987), the borate dissociation constant from Lyman (1975) with B:S value of Uppstrom (1974) and the CO_2 solubility from Weiss (1974). Precision was about ± 10 μM for DIC and ± 10 ppm for pCO_2.

The $\delta^{13}C$-DIC measurements were performed according to the method described by Gillikin and Bouillon (2007): a headspace was created in 100 mL sealed glass bottles by injecting a volume of helium equivalent to about 30% of the total vial volume. Samples were then acidified with 0.3 mL of 85% phosphoric acid to convert DIC species into CO_2. After shaking and equilibrating for more than one night at the thermostated room temperature of the mass spectrometer laboratory, samples were analysed using a dual inlet EA-IRMS (EA: Carlo Erba NC2500; IRMS: Isoprime). About 0.5 mL of headspace was injected through an injection port that was placed before the water trap of the EA. The $\delta^{13}C$ values were calibrated with a homemade standard (45 mg of Na_2CO_3 dissolved with 3 mL of 85% phosphoric acid in a 100 mL helium flushed vial) whose isotopic composition was previously determined to be -4.5 ± 0.2 ‰ (Polsenaere et al., 2013). The $\delta^{13}C$ of the total DIC was computed using these corrected

330 $\delta^{13}C$ values and the equation of Miyajima (1995), which defines the partitioning of CO_2
331 between the headspace and the water phase of the sample as a function of temperature and
332 salinity. The precision of these measurements was estimated at about ± 0.1 ‰, based on
333 replicate analyses of the same samples.
334
335 3. Results
336
337 3.1. Surface seawater
338
339 The practical salinity (S_P) of surface seawater at the beach was 35.1 ± 0.4 (s.d., n = 37)
340 and oxygen saturation close to 100% (98 ± 4.5% s.d.) throughout the year. The pH (on the
341 infinite dilution convention or "NBS" scale) ranged from 8.10 to 8.30, whereas temperature
342 displayed a seasonal variation with values ranging from 8.0 – 13.9°C in winter, to 11.3 – 18.9°C
343 in spring, 18.4 – 21.9°C in summer and 14.1 – 20.1°C in autumn (Table 1 in supplementary
344 material). DOC concentrations varied between 84 and 600 μM, with an average concentration
345 of 260 ± 150 μM (n = 37) and maximum values observed during spring and summer (Fig. 3).
346 TA values ranged from 2100 to 2480 μmol kg^{-1}, with a mean value of 2310 ± 110 μmol kg^{-1} (n
347 = 37) and minimum observed values in winter. Calculated DIC and pCO_2 values ranged,
348 respectively, from 1900 to 2300 μM (average value of 2070 ± 102 μM; n = 37) and from 300
349 to 526 ppm (average value of 395 ± 63 ppm; n = 37), and displayed a similar trend, with minima
350 observed during autumn and winter. The $\delta^{13}C$-DIC was relatively constant, with a mean value
351 of +0.4 ± 0.5 ‰ (n = 37) (Fig. 3).
352
353 3.2. Intertidal beach pore waters
354
355 Irrespective of the season, pore waters collected at the surface of the intertidal beach
356 water table had a salinity close to that of seawater, with 80% of samples having a practical
357 salinity between 34 and 36. Nevertheless, several samples collected in the lower beach had
358 salinities as low as 30, with a minimum value of 25.6 on April 19th, 2011 (Fig. S1 in
359 Supplementary material for detailed cross-shore profiles). In the upper beach (between 30 and
360 70 m from the dune foot), pore waters retrieved from deep holes had chemical characteristics
361 close to those of seawater (Fig. 3). Dissolved oxygen saturation was between 100% and 80%
362 and pCO_2 values were close to atmospheric, with a mean of 455 ± 113 ppm (n = 37). DIC

363 concentrations were below 2300 μM, with a mean value of 2120 ± 170 μM (n = 37). The δ^{13}C-
364 DIC had a mean value of 0.0 ± 1.0‰ (n = 37) (Fig. 3). Pore water DOC concentrations in the
365 upper beach were higher than those of seawater, with values up to 840 μM (April 19th, 2011)
366 and a mean concentration of 310 ± 180 μM (n = 37) (Fig. S2 in Supplementary material for
367 average values).
368 In the lower beach, pore waters were generally depleted in oxygen and enriched in DIC,
369 including the highest pCO_2 and lowest δ^{13}C-DIC values along the cross-shore transects (Fig.
370 3). Pore waters characteristics along the cross-shore transects varied throughout the year:
371 minimum oxygen saturations ranged from 22% to 86% in winter (average value of 55 ± 23%,
372 n =10), from 3% to 50% in spring (average value of 36 ± 22%, n = 8), from 0% to 58% in
373 summer (average value of 23 ± 20%, n = 13) and from 9% to 72% in autumn (average value of
374 44 ± 23%, n = 6) (Fig. S2 in Supplementary material for seasonal average values). Maximum
375 DIC values also varied seasonally. For samples with salinity close to that of seawater, the DIC
376 concentrations of the most oxygen-depleted pore waters ranged from 1950 to 2510 μM in winter
377 (average value of 2130 ± 130 μM, n = 10), from 2210 to 2550 μM in spring (average value of
378 2360 ± 90 μM; n = 8), from 2190 to 2600 μM in summer (average value of 2340 ± 130 μM, n
379 = 13) and from 2020 to 2350 μM in autumn (average value of 2180 ± 120 μM, n = 6) (Fig. 3).
380 The computed pCO_2 displayed the same trend: the highest values were observed during
381 summer, ranging from 610 to 1520 ppm (average value of 1040 ± 200 ppm, n = 13). During the
382 rest of the year, pCO_2 values of lower beach pore waters ranged from 350 to 960 ppm in winter
383 (average value of 540 ± 190 ppm, n = 10), from 610 to 1420 ppm in spring (average value of
384 870 ± 260 ppm, n = 8), and from 520 to 1010 ppm in autumn (average value of 720 ± 230 ppm,
385 n = 6).
386 Pore water δ^{13}C-DIC values were almost always more negative in the lower beach than
387 in the upper beach (Fig. 3). The lower beach values ranged from -2.7 to +0.3‰ in winter
388 (average value of -0.9 ± 0.9‰, n = 10), from -3.9 to -0.8‰ in spring (average value of -1.8 ±
389 1.1‰, n = 8), from -3.4 to -0.3‰ in summer (average value of -1.4 ± 0.9‰, n = 13) and from
390 -1.7 to -0.1‰ in autumn (average value of -0.8 ± 0.6‰, n = 6).
391 Pore water DOC concentrations along the cross-shore profile displayed no uniform
392 trend: 21 out of the 37 completed profiles showed DOC values higher in the upper beach than
393 in the lower beach; 14 transects showed uniform or scattered DOC values along the cross-shore
394 profile. An increase in DOC concentration in the lower beach was observed on 02/22/2011 and
395 05/19/2011 (Fig. 1 in Supplementary material). On the 21 dates when DOC concentrations were

decreasing from the upper beach to the lower beach, most of the decrease was observed in the upper part of the intertidal zone and DOC concentrations were often lower than 300 μM in the lower beach pore waters (mean value of 220 ± 140 μM, n = 37), except from May to August 2012 when high DOC concentrations were observed along the whole cross-shore profile (mean value of 520 ± 100 μM, n = 50). When pore water DOC concentrations displayed no cross-shore trend, they typically ranged from 150 to 200 μM (Fig. 1 in Supplementary material).

3.3. Supratidal wells

The three piezometers placed between the dune foot and the high tide mark allowed us to sample waters from the surface beach aquifer at low tide over a full lunar tidal cycle in February-March 2013 and September-October 2013. The hydraulic head measurements revealed that pore waters flowed seaward, i.e., from PZ1 (dune foot) to PZ3 (high spring tide watermark), except during the high spring tides (Fig. 4A) when waves reached the PZ3 position and surface seawater percolated through the sand. This lead to a brief inversion of the hydraulic gradient, with the water table being higher in PZ3 than in PZ2 and PZ1.

The pore water salinity changed according to the tidal cycle. The piezometer (PZ3), located at the high spring tide water line, contained saline water (S_P ~ 34.5) during spring tide periods and brackish waters (S_P ranging from 0 to 5) during neap tide periods (Fig. 4). The other piezometers (PZ1 and PZ2), located a few meters upstream, contained fresh to brackish waters, with S_P lower than 15 (Fig. 4).

Due to the limited availability of sensors, oxygen saturation was measured only in PZ2 and PZ3. The data show that pore waters were depleted in oxygen during neap tides, with values ranging from 11 to 48% in February-March and from 0 to 10% in September-October in PZ2, and ranging from 22 to 63% in February-March and from 48 to 71% in September-October in PZ3 (Fig. 4B). Pore waters were more oxygenated during spring tides because of saline water intrusion, with values ranging from 85 to 100%, except for PZ2 in September-October as saline waters did not reach this station.

Pore water DIC concentrations, calculated from TA and pH measurements carried on samples recovered at low tide, were higher in the freshwater of PZ1 than in the fresh to saline waters of PZ2 and PZ3, with values in PZ1 ranging from 2780 to 4080 μM (average value of 3570 ± 380 μM, n =17), with no particular trend throughout the lunar tidal cycle (Fig. 4B). In contrast to PZ1, in PZ2 and PZ3, DIC concentrations evolved concomitantly with salinity, i.e.,

to the lunar tidal cycle. The DIC concentrations were higher in the fresh-brackish pore waters of PZ2 and PZ3 during neap tides than in saline waters during spring tides. In PZ3, freshwater DIC values ranged from 2780 to 3070 μM (average value of 2880 ± 100 μM, n =7) in February-March, and from 3020 to 3480 μM (average value of 3160 ± 150 μM, n =7) in September-October. In PZ2, DIC values ranged from 3000 to 3380 μM (average value of 3220 ± 170 μM, n =8) in February-March, and were nearly invariant at ~3800 μM in September-October when salinity remained close to 0. During spring tides, the mean DIC concentrations were 2130 ± 130 μM (n = 5) for both seasons in PZ3, and 2780 ± 160 μM (n = 4) in PZ2 for the February-March sampling (Fig. 4B).

Pore water pCO_2 displayed a similar trend to DIC in all three piezometers and during both sampling campaigns, with high values during neap tides and lower values during spring tides. In February-March, pCO_2 values in PZ1 ranged from 1000 to 1770 ppm (average value of 1330 ± 390 ppm, n = 3) during spring tide, whereas two higher values (1690 and 2820 ppm) were observed during neap tide. In PZ2, the mean pCO_2 was 780 ± 15 ppm (n = 3) during spring tide and ranged from 520 to 2030 ppm (average value of 1460 ± 550 ppm, n = 6) during neap tide. The same trend was observed in PZ3, with pCO_2 ranging from 365 to 448 ppm during spring tide (mean value of 413 ± 38 ppm, n = 4) and 354 to 974 ppm during neap tide (mean value of 510 ± 240 ppm, n = 6) (Fig. 4B). In September-October, average pCO_2 values in PZ1, PZ2 and PZ3 were respectively 2780 ± 250 (n = 4), 2130 ± 800 (n = 4) and 770 ± 70 (n = 4) ppm during spring tide, and about 3510 ± 1310 (n = 4), 3140 ± 810 (n = 6) and 1010 ± 260 (n = 5) ppm during neap tide (Fig. 4B). The pore water $\delta^{13}C$-DIC values changed with the salinity, ranging from -9.9 to -12.2‰ in fresh and brackish waters to -3.8‰ in saline waters (Fig. 4A).

3.4. Terrestrial groundwater

Waters collected in upland, forest wells, above the Truc Vert Beach, were fresh ($S_P \approx 0$) and always anoxic. In all these wells, the water table was about 3.2 to 3.5 m NGF (French national reference levelling) higher than in the upper beach (1.6 to 2.5 m NGF), evidence of a groundwater hydraulic gradient from the upland to the beach. The pH of these terrestrial groundwaters was circum-neutral, with pH values ranging from 6.27 to 7.53 (Table 1). DOC concentrations ranged from 1060 to 2320 μM, except in DFCI 2 where higher DOC concentrations were observed (3170 and 5800 μM; Table 1). The average DIC concentration in the forest wells was 4700 ± 1100 μM (n = 12). DIC concentrations varied between wells but

462 also with time, as observed in well DFCI2 in which DIC was 2120 μM in Sept. 2013 and 6180
463 μM in Jan. 2014 (Table 1). Despite this temporal variability, the DIC concentrations of the
464 terrestrial groundwaters in the upland wells were generally higher than in the beach pore waters.
465 Likewise, the aqueous pCO_2 was much higher in forest wells than in beach pore waters, and
466 ranged from 5200 to 82000 ppm in the former (Table 1). The highest value (82000 ppm),
467 calculated from the total alkalinity, in-situ pH and temperature, is probably an overestimate due
468 to the acidic and organic-rich nature of the waters in well DFCI2 (pH of 6.27; DOC content of
469 3170 μM) (Abril et al., 2015). The computed pCO_2 in the other wells, in which pH was always
470 close to 7 and DOC concentrations always lower than 2350 μM (average value of 1700 ± 470
471 μM, n = 9), are more uniform (Table 1). If we exclude the anomalous high value at DFCI2, the
472 mean pCO_2 in forest wells was 16500 ± 6500 ppm (n = 11), which was two- to five-fold higher
473 than pCO_2 values calculated in the beach pore waters. The δ^{13}C-DIC values were always very
474 negative in the upland wells, ranging from -22.5 to -13.9‰ (average value of -16.9 ± 2.2‰).
475
476 4. Discussion
477
478 4.1. DIC transformation below the foredune
479
480 Most tidal beaches host a redox front along the salinity gradient between terrestrial fresh
481 groundwaters and saline pore waters (Windom and Niencheski, 2003; Slomp and Van
482 Cappellen, 2004; Spiteri et al., 2008; Santos et al., 2009). This redox transition zone is the site
483 of biogeochemical transformations linked to the oxidation, by oxygenated seawater, of reduced
484 compounds dissolved in fresh groundwater. For example, the oxidative precipitation of
485 dissolved iron at the redox front can create a trap for solutes, such as orthophosphate and trace
486 metals, that are co-precipitated with or adsorbed to the authigenic oxides (Cable et al., 2002;
487 Charette and Sholkovitz, 2002; Slomp and Van Cappellen, 2004; Spiteri et al., 2008). The
488 terrestrial fresh groundwater sampled in the forest, upland of the Truc Vert Beach, were anoxic
489 and enriched in Fe(II) and NH_4^+ (Table 2). Dissolved Fe(II) and NH_4^+ concentrations were
490 measured in the upland wells (59 ± 30 μM and 17 ± 18 μM, respectively), whereas these species
491 were nearly absent in the dune foot freshwater end-member (0.1 ± 0.2 μM and 0.5 ± 1.4 μM,
492 respectively) (Table 2; Anschutz et al. 2016). Unlike most other STEs, the salinity gradient in
493 the supratidal beach did not host a redox gradient. Since freshwaters of the surficial aquifer at
494 the dune foot are oxic, the oxic-anoxic front must occur in the freshwater aquifer below the
495 foredune. The foredune at the Truc Vert Beach is a wide (up to 200 m), sandy and organic soil-

depleted area. It is believed that rainwater can percolate through the sand dune and bring oxygen to the shallow, fresh groundwaters (Anschutz et al., 2016). In addition, the groundwater TA was higher in the forest than in the upper beach and this may reflect the impact of local redox reactions that serve as sources or sinks of alkalinity (Kempe, 1990; Stumm and Morgan, 1996; Abril and Frankignoulle 2001; Thomas et al., 2009). The oxidation of reduced Fe and nitrification of ammonia by oxygen consumes alkalinity (Eqns. 1 and 2) (Stumm and Morgan, 1996; Abril and Frankignoulle, 2001; Burdige, 2006):

$$4Fe^{2+} + O_2 + 8HCO_3^- + 2H_2O \rightarrow 4Fe(OH)_3 + 8CO_2 \quad (1)$$

$$NH_4^+ + 2O_2 + 2HCO_3^- \rightarrow NO_3^- + 2CO_2 + 3H_2O \quad (2)$$

According to the stoichiometry of these reactions, the oxidation of the anoxic groundwater iron and ammonia would have removed 152 µM of TA, very close to the difference we measured at the two sites (142 µM; Table 2). Hence, these TA values clearly support the hypothesis of the presence of a redox front located below the foredune. Hydrologic mass balance calculations yield an annual flux of terrestrial SGD of 0.43 km^3. Accordingly, the flux of alkalinity to the coastal ocean would be 1.54 Gmol per year for the whole Aquitaine coast, based on the properties of the forest well end-member. The value is reduced to 1.47 Gmol per year because of oxidation reactions below the foredune.

Protons released by the redox reactions (Eqns. 4 and 5) should decrease TA and pH, but increase the pCO_2. In contrast, we observe a lower pCO_2 in the oxic dune foot aquifer than in the anoxic forest aquifer and these lower pCO_2 values are accompanied by higher pHs, lower DIC concentrations and heavier δ^{13}C-DIC values (Table 2). These observations suggest that CO_2 degasses into the interstitial air of the dune sands and finally to the atmosphere. As CO_2 progressively degasses along the groundwater flow path, the δ^{13}C-DIC increases due to the preferential diffusion of $^{12}CO_2$ (Mook et al., 1974; Cerling et al., 1991; Polsenaere and Abril, 2012; Deirmendjian and Abril, 2018) while DIC decreases and the pH increases (Fig. 5).

Discharge of terrestrially-derived CO_2-enriched groundwater may modify the pH of the coastal ocean and locally influence ocean acidification (Cai et al., 2003). When the groundwater DIC:TA ratio is greater than 1, groundwater discharge may decrease seawater pH, whereas a DIC:TA ratio <1 will buffer seawater against ocean acidification (Pain et al., 2019). Terrestrial groundwater sampled in forest wells have a DIC:TA ratio above 1 (Tab. 2), mostly because of high pCO_2 values. Along the groundwater flow path, TA decreases due to oxidation of reduced iron and ammonium while DIC decreases due to CO_2 degassing. The latter has a larger

influence on the TA:DIC ratio than the former, as the ratio evolves towards 1 in supratidal fresh groundwater and ultimately becomes lower than 1 in brackish waters (Tab. 2, Fig. 5). Accordingly, terrestrial SGD at the Truc Vert Beach will not lower pH in receiving seawater, unlike most other coastal environments where DIC fluxes have been investigated so far (de Weys et al., 2011; Cyronak et al., 2014; Sadat-Noori et al., 2016; Liu et al., 2017; Mouret et al., 2020). Seawater pH may also increase due to enhanced biological productivity buoyed by a SGD-derived nutrient flux (Borges and Gypens, 2010), which consist mostly of a nitrate flux at the Truc Vert Beach (Anschutz et al., 2016). Therefore, both the DIC:TA ratio and nutrient fluxes of SGD result in an increasing seawater buffering capacity against acidification in this high-energy beach.

4.2. DIC behavior in the subterranean estuary

4.2.1. Non-conservative behavior of DIC in the STE

Terrestrial groundwaters are a source of nutrients, trace metals, and carbon to the coastal ocean (Burnett et al., 2003; Bowen et al., 2007; Santos et al., 2009, 2012b). In permeable beaches, the reaction zone between terrestrial groundwaters and saline pore waters forms the STE (Moore, 1999). As observed in surface estuarine systems, terrestrial groundwater undergoes chemical transformations in the STE before discharging to the coastal ocean. Multiplying the average elemental concentration by the subterranean freshwater flux often provides inaccurate estimates of mass fluxes to the coastal ocean for species like nutrients and carbon that do not behave conservatively in the STE (Charette and Sholkovitz, 2002; Slomp and Van Cappellen, 2004; Beck et al., 2007; Chaillou et al., 2016; Liu et al., 2017). In the Truc Vert Beach, geophysical measurements coupled to hydraulic head and salinity measurements reveal that the subsurface salinity gradient is located in the supratidal beach and is a few meters wide. The fresh-saline interface is almost vertical and shifts only a few meters cross-shore during the spring-neap tidal cycle, implying that the transition zone between fresh and saline groundwaters is relatively narrow and stable (Buquet et al., 2016). The PZ3 piezometer was located in this transition zone. Electrical resistivity tomographic measurements also show that the tidally-driven seawater recirculation cell drags parcels of brackish water from the supratidal transition zone toward the lower beach (Fig. 2) (Buquet et al., 2016), which explains why we sampled brackish pore waters in piezometers located in the supratidal beach as well as in holes of the lower beach. High DIC concentrations and pCO_2 in the freshwater end-member from forest wells (Table 1) originate from autotrophic root respiration and from carbon fixed by

terrestrial plants, then recycled within soils through heterotrophic respiration, and finally transferred to the groundwater (Hanson et al., 2000; Cole et al., 2007). Fresh groundwater was also sampled in piezometers at the foot of the dune, but the measured δ^{13}C-DIC and computed DIC and pCO_2 values were dissimilar those in waters from forest wells (Table 2).

The behaviour of DIC and δ^{13}C-DIC in the STE, i.e. in brackish waters of the supratidal and lower beaches, can be assessed by comparing results of end-member, conservative mixing and field data (Fry, 2002; Bouillon et al., 2003). The equation describing conservative mixing of DIC in the salinity (S) gradient is given by:

$$DIC = \left(\frac{DIC_{SW} - DIC_{FW}}{S_{SW} - S_{FW}}\right) S + DIC_{FW} \qquad (3)$$

where subscripts refer to the seawater (SW) and freshwater end-members (FW). Theoretical DIC concentrations were calculated using the two freshwater end-members observed in the immediate vicinity of the Truc Vert Beach: fresh forest groundwaters (salinity of 0; average DIC of 4700 µM) and supratidal fresh pore waters (average salinity of 0.6; average DIC of 3500 µM). The seawater end-member properties correspond to the average salinity and DIC concentration of the local surface seawater (35.1 and 2070 µM, respectively). The equation describing the conservative mixing of δ^{13}C-DIC was derived by Bouillon et al. (2003) and is:

$$\delta^{13}C = \frac{S(DIC_{FW}\delta^{13}C_{FW} - DIC_{SW}\delta^{13}C_{SW}) + S_{FW}DIC_{SW}\delta^{13}C_{SW} - S_{SW}DIC_{FW}\delta^{13}C_{FW}}{S(DIC_{FW} - DIC_{SW}) + S_{FW}DIC_{SW} - S_{SW}DIC_{FW}} \qquad (4)$$

As S_{FW} is 0, equation (4) simplifies to

$$\delta^{13}C = \frac{S(DIC_{FW}\delta^{13}C_{FW} - DIC_{SW}\delta^{13}C_{SW}) - S_{SW}DIC_{FW}\delta^{13}C_{FW}}{S(DIC_{FW} - DIC_{SW}) - S_{SW}DIC_{FW}} \qquad (5)$$

where δ^{13}C represents the carbon isotopic composition of the DIC. δ^{13}C end-members were defined as +0.4‰ for seawater, -16.9‰ for the terrestrial groundwater, and -12.1‰ for the supratidal freshwaters.

Irrespective of the freshwater end-member, results of the calculations clearly show that DIC does not behave conservatively along the salinity gradient (Fig. 6). In the supratidal beach brackish waters, DIC concentrations were below the theoretical mixing lines, indicating that DIC was depleted (Fig. 6A). The δ^{13}C-DIC values from these samples were markedly higher

than predicted (Fig. 6B). Carbonate dissolution cannot explain this trend as it would increase the DIC beyond the mixing line. The combination of decreasing DIC and increasing δ^{13}C-DIC, coupled with lower pCO_2 values in brackish waters ($S_P > 1$) than in freshwaters ($S_P < 1$), is best explained by CO_2 degassing at the interstitial water – interstitial air interface in the supratidal STE.

In the brackish pore waters of the lower beach, DIC concentrations were either on or above the mixing lines between the supratidal-beach freshwaters and seawater (Fig. 6A). Most of the δ^{13}C-DIC data were close to the theoretical mixing line (Fig. 6B). More negative δ^{13}C-DIC values, coupled to enriched DIC concentrations, suggest the presence of a source of metabolic carbon from organic matter mineralization, as proposed in section 4.3. The DIC in the STE of the Truc Vert Beach was therefore controlled by two main processes: CO_2 degassing along the salinity gradient in the supratidal and upper beach, and organic matter respiration within the intertidal zone. A few samples with higher than expected δ^{13}C-DIC values and enriched in DIC suggest that some carbonate dissolution may also occur (see detailed discussion in section 4.3.4).

4.2.2. Fluxes of carbon from the freshwater end-member

Mixing between fresh and saline pore waters was observed during neap tides, when low salinities (from 1 to 2) were observed in PZ2 and PZ3. pH and δ^{13}C-DIC increased from PZ1 ($S_P = 0.6$) to PZ3 ($S_P \sim 2$), whereas pCO_2 decreased from 2340 to 770 ppmv (Table 2). The high mean pH value of 8.31 observed in these nearly freshwaters corresponded to the value computed from electroneutrality at in-situ pCO_2, temperature, and measured TA. The increase in pH from the upland groundwater to the beginning of the salinity gradient of the supratidal beach STE suggests that CO_2 was degassing to the atmosphere below the foredune and in the STE, and implies that the upland aquifer cannot be used as a freshwater end-member to calculate fluxes of carbon from terrestrial SGD (Fig. 5). The loss of DIC due to CO_2 degassing below the dune between the forest soil aquifer and the supratidal beach is about 1550 µM. This corresponds to a yearly flux of about 8000 tons of C (or 29000 tons of CO_2) to the atmosphere when extrapolated over the whole Aquitaine sandy coast. Given that the average DIC concentration of these waters after degassing below the dune is 3150 µM (Table 2), the DIC flux to the coastal ocean is estimated at 16200 tons of carbon per year. It would have been overestimated by 8000 tons per year if active CO_2 degassing between the forest soil aquifer and the supratidal beach had been neglected.

630
631
632 4.3. Carbon behaviour in the beach aquifer
633
634 4.3.1. Aerobic respiration within the intertidal recirculation cell
635
636 High-energy sandy beaches are recognized as environments in which organic matter
637 mineralization and recycling of the associated nutrients are very active (Avery et al., 2008;
638 Rauch et al., 2008; Rocha, 2008; Anschutz et al., 2009; Dugan et al., 2011; Charbonnier et al.,
639 2013). Previous studies at the Truc Vert Beach revealed that oxygen consumption through
640 aerobic respiration takes place in the intertidal recirculation cell (Anschutz et al., 2009;
641 Charbonnier et al., 2013). Oxygenated seawater seeps into the sandy sediments during floods,
642 filling the pore space. As seawater percolates from the upper beach to the lower beach, oxygen
643 is partly consumed through aerobic respiration and, ultimately, oxygen-depleted pore waters
644 are expelled from the sand and are flushed to the coastal ocean when the lower beach is exposed
645 (Charbonnier et al., 2013). Thus, the pore water of the upper beach is young as it has just entered
646 the aquifer, whereas the water in the lower beach has percolated into the aquifer and is therefore
647 older. The residence time of pore water in the beach aquifer is between 7 and 20 tidal cycles,
648 as inferred from dissolved silica concentrations and experimental measurements of quartz
649 dissolution (Anschutz et al., 2009). This suggests that the pore water volume was renewed
650 during our bi-weekly samplings. Hence, the pore water of a given cross-shore profile was not
651 the same as that sampled on our previous visit 15 days before.
652 Partially oxygen-depleted pore waters in the lower beach are also enriched in DIC (Fig.
653 3). In fact, the highest DIC and pCO_2 values are associated with the most O_2-depleted pore
654 waters (Fig. 3), implying that DIC is mostly produced by aerobic respiration processes within
655 the intertidal sands (Charbonnier et al., 2013). Temperature differences, between seawater
656 entering the aquifer during the rising tide and the pore water that seeps out the aquifer in the
657 lower beach, were for most profiles less than 1°C (22 out of 37). The largest temperature
658 difference was 2.2°C, which leads to a 10% differential on the computed pCO_2 values (+4.23%
659 $°C^{-1}$; Takahashi et al., 1993). Temperature differences arose as we sampled pore waters close
660 to the surface in the lower beach and, thus, they were influenced by the air temperature. The
661 largest temperature differences were observed in summer, when the computed pCO_2 is highest.
662 The temperature differential translates into a 100 ppm change in pCO_2 when their values at in

663 situ temperature exceed 1000 ppm (Fig. 3). Irrespective, the impact of temperature on computed
664 pCO_2 values are minor compared to those resulting from microbial respiration.
665 Most of cross-shore transects performed in 2011-2012 showed that oxygen depletion
666 and the concomitant DIC enrichment in the lower beach pore waters are coupled with a decrease
667 in DOC concentrations along the transects (Fig. 3; Fig. 1 in Supplementary material). DOC
668 concentrations were higher in upper beach pore waters than in the local seawater on most
669 sampling dates, but especially in the spring and summer. During these two seasons, the upper
670 beach pore waters contained, on average and respectively, 140 and 60 μM more DOC than the
671 seawater (Fig. 3), but they could be a few hundred μM higher on any given day (Fig. 1 in
672 Supplementary material).
673 DOC is a key intermediate in benthic POC catabolic processes (Kristensen and Hansen,
674 1995; Komada et al., 2012). DOC can be produced through cells lysis and/or bacterial
675 enzymatic activity, and be consumed through heterotrophic respiration (Carlson and Hansell,
676 2014). The DOC concentration gradients observed along the transects likely result from a
677 balance between these two processes. Our data suggest that DOC production dominates in the
678 upper part of the Truc Vert Beach. The DOC in excess of the local seawater contribution most
679 likely originates from the degradation of fresh marine POC, including scattered, drifting plant
680 debris and phytoplankton cells (Huettel and Rusch, 2000), that are filtered and trapped by the
681 sand as seawater percolates through it during rising tides. As pore waters percolate seaward
682 through the beach aquifer, DOC is consumed by heterotrophic aerobic respiration and its
683 concentration decreases to a value similar to that measured in open seawater. This background,
684 residual DOC is probably more refractory, as the concentration remained relatively stable
685 despite its transit in the aquifer aerobic reactor. Given the limited amount of labile organic
686 carbon and the constant renewal of dissolved O_2 through seepage, heterotrophic processes
687 remain strictly aerobic. Accordingly, carbon and alkalinity fluxes are not affected by anaerobic
688 processes, unlike most other coastal permeable environments studied to date (e.g. Cai et al.,
689 2003; Liu et al., 2017). Because DOC concentrations in lower beach pore water are similar to
690 those of the local seawater, pore waters discharging from the Truc Vert Beach are apparently
691 not a source of DOC to the coastal ocean, in contrast to less energetic beaches and tidal flats
692 worldwide (Goñi and Gardner, 2003; Santos et al., 2009; Avery et al., 2012; Kim et al., 2012;
693 Goodridge, 2018). Hence, irrespective of the season, carbon is mostly exported to the coastal
694 ocean as DIC.
695
696

4.3.2. Fluxes of carbon from tidally-driven seawater recirculation

The mean DIC enrichment in saline pore waters (S_P > 34.5) was 144 μM, as derived from the difference between concentrations in the lower beach pore waters and seawater (Fig. 3). Considering the volume of pore water exchanged between the beach and the coastal ocean during each tide (15.2 m^3 per longshore meter; Charbonnier et al., 2013), the DIC export is 1500 moles of carbon per longshore meter per year. If we extrapolate over the 240-km long Aquitaine coast, the DIC flux, from aerobic respiration of marine organic matter in intertidal sands, to the coastal ocean is about 360 Mmol (4400 tons) of carbon per year. This value is of the same order of magnitude as the 3500 tons of mineralized carbon calculated by Charbonnier et al. (2013) from Redfield ratios and the pore water oxygen deficit.

Part of the metabolic DIC is delivered by SGD in the form of dissolved CO_2, as pH decreases and pCO_2 increases from the upper to the lower beach, with a mean enrichment of about 300 ppm relative to the atmosphere and discrete values reaching as high as 1500 ppm (Fig. 3). Consequently, CO_2 degassing to the atmosphere may occur. In fact, we observed bubbles being expelled from the sands in the swash zone when the first waves of the flooding tide filled the intertidal sands with seawater. These bubbles originated from air trapped in the sediment during sediment desaturation at low tide. This mechanism would favour CO_2 degassing, as CO_2 can diffuse from the pore waters to interstitial air in the unsaturated sand at low tide and the interstitial air is expulsed to the atmosphere during rising tides.

4.3.3. Fluxes of carbon compared to other coastal systems

Given a mean intertidal beach width of 150 m, the calculated DIC flux from seawater recirculation is 27 mmolC m^{-2} d^{-1}. The total DIC flux, including the terrestrial groundwater flux is 130 mmolC m^{-2} d^{-1}. The calculated flux is not large enough to significantly affect the DIC inventory of the open ocean coastal waters because it is incremental with respect to the flow of seawater at the coast driven by coastal currents that characterize the Bay of Biscay continental shelf. The calculated DIC flux is much lower than fluxes from SGD affected by a strong input of fresh groundwaters from organic-rich environments, such as mangroves, estuaries, lagoons, or salt marshes (Sadat-Noori et al., 2016 and references therein; Table 3). Nevertheless, it stands in the high range of f DIC fluxes calculated for advective pore water fluxes in marine permeable sediments (Cook et al., 2007; Cyronak et al., 2013; Faber et al., 2014).

731 4.3.4. DIC isotopic signatures in intertidal pore waters
732
733 The isotopic signature of the DIC can be used to distinguish qualitatively and
734 quantitatively its origin (Bouillon et al., 2007; Miyajima et al., 2009). For saline pore waters of
735 the lower beach (S_P > 34.5), the δ^{13}C-DIC was linearly correlated with the consumption of
736 dissolved oxygen (r^2=0.37, N=265) as a result of the predominant aerobic respiration within the
737 sands (Fig. 7A). A similar trend was observed for the brackish pore waters of the lower beach
738 (S_P < 34.5), but some samples clearly fall outside the general trend (Fig. 7A). In fact, four
739 groups of intertidal pore waters could be distinguished on the basis of the δ^{13}C-DIC behaviour
740 along the salinity gradient (S_P ~25-36) of the lower beach (Fig. 7B). Combined to their DIC
741 and oxygen contents, these four groups of pore waters highlight the different processes at play
742 in the intertidal sands of the Truc Vert Beach: conservative mixing of fresh and saline waters,
743 aerobic respiration, and carbonate dissolution (Fig. 7). For each group of pore waters, a Keeling
744 plot (δ^{13}C-DIC versus 1/DIC) was drawn to determine the δ^{13}C signature of the predominant
745 DIC source (Keeling, 1958, Pataki et al., 2003).
746 The first group of water (group A) corresponds to saline (S_P > 34.5), oxygen-depleted
747 and DIC-enriched pore waters with δ^{13}C-DIC values between +0.5 and -1.22‰, waters whose
748 variable properties are attributed to aerobic respiration of organic matter within the intertidal
749 saline plume (Anschutz et al., 2009; Charbonnier et al., 2013). The slope of the linear
750 regressions is similar for every season (Fig. 7C), but the range of 1/DIC values evolves with
751 time as the DIC concentration of the surface seawater (and TA; Fig. S3 in Supplementary
752 material) changed seasonally (Fig. 3 and 7C). The slope of the TA vs DIC for the surface
753 seawater in all seasons is 1.02 with r^2 = 0.865 (Fig. S4 in Supplementary material), suggesting
754 that biogenic carbonate precipitation in coastal waters explains seasonal changes of these
755 parameters. Irrespective of the season, the isotopic composition of the DIC added to seawater,
756 as derived from the y-intercept of the regression line, ranges from -19.1 to -15.8‰ (Fig. 7C),
757 consistent with an addition of metabolic CO_2 from the mineralization of marine organic matter
758 (Mook, 2000).
759 The second group of waters (group B) corresponds to few DIC-enriched brackish pore
760 waters characterized by δ^{13}C-DIC values higher than predicted from conservative mixing. The
761 combination of high δ^{13}C-DIC values with a DIC (and TA, Fig. S3 in Supplementary material)
762 enrichment is indicative of carbonate dissolution. The y-intercept of the Keeling plot is about
763 +1.8‰ (Fig. 7D), in agreement with the proposed marine calcium carbonate origin (0 to +2‰;

Mook, 2000). The $CaCO_3$ content of the sands is up to 3.7 wt% in the lower part of the beach (Charbonnier et al., 2013). It consists of calcite and aragonite shell debris. The accumulation of metabolic CO_2 in this system, resulting from catabolic aerobic processes, could lower the saturation stage of the pore water and trigger the dissolution of the most soluble $CaCO_3$ polymorph, aragonite. This hypothesis, inferred from δ^{13}C-DIC values, could be tested by measurements of dissolved calcium concentrations (e.g. Cai et al., 2003).

The third group of waters (group C) corresponds to the brackish pore waters. These are characterized by conservative δ^{13}C-DIC values and little oxygen depletion (O_2 saturation > 85%). The y-intercept of the Keeling plot for these waters yields an isotope signature of -12.0‰ for the DIC source (Fig. 7E), which corresponds to the δ^{13}C-DIC of the fresh groundwater end-members collected in piezometers of the supratidal beach (Table 2). These samples most likely correspond to a simple mixture of freshwaters with seawater, unaltered by other processes like respiration or carbonate dissolution.

The last group of pore waters (group D) consists of DIC-enriched, O_2-depleted (consumed O_2 > 100 μM) brackish pore waters with low δ^{13}C-DIC. These waters are affected by mixing between upper-beach freshwaters and seawater as well as respiration processes. In these brackish waters, the respired organic matter can be either marine (entering sands during high tide with seawater) or terrestrial (brought as DOC in fresh groundwaters). The Keeling plot indicates that the isotope carbon composition of this last DIC source is about -16.5‰ (Fig. 7F), akin to organic matter of marine origin (Mook, 2000). Given the possible temporal variability of DIC sources, we estimated the δ^{13}C signature of the respired carbon source for each pore water of group D using the following equation (Bouillon et al., 2003):

$$\delta^{13}C_{added} = \frac{DIC_{MEAS}\delta^{13}C_{MEAS} - DIC_{MX}\delta^{13}C_{MX}}{DIC_{MEAS} - DIC_{MX}} \qquad (6)$$

where $\delta^{13}C_{added}$ is the carbon isotope composition of added DIC, considering that DIC enrichment originated solely from organic matter respiration. $\delta^{13}C_{MEAS}$ and DIC_{MEAS} are, respectively, the DIC concentration and isotopic composition of each sample; $\delta^{13}C_{MX}$ and DIC_{MX} correspond to the computed δ^{13}C-DIC and DIC values for conservative mixing between the supratidal beach fresh groundwater and seawater.

This approach yields a wider range of DIC sources, with $\delta^{13}C_{added}$ values ranging from -19.0 to -4.8‰ (Table 4). This range of values is far from those of land sources, such as terrestrial higher plants that characterize the forest upland of the Truc Vert Beach (-28‰± 1.3;

797 Dubois et al., 2012). The heavier $\delta^{13}C_{added}$ values can originate from C4 plants (Ehleringer et
798 al., 1986; Mook, 2000) such as dune grasses. Most (7 out of 9) of the samples yielded $\delta^{13}C_{added}$
799 values ranging from -19.0 to -9.3‰, corresponding to marine organic matter (Mook, 2000) and
800 C3 seagrasses (Andrews and Abel, 1979). In the study area, plants with this isotopic signature
801 can be marine phytoplankton and drifting plant debris (also known as wracks) such as Zostera
802 marina or Zostera noltei (-11‰±2; Dubois et al., 2012), dispersed on the beach at the high tide
803 water line. Aerobic respiration in the intertidal aquifer of the Truc Vert Beach is thus mainly
804 fuelled by marine organic matter. Degradation of terrestrial organic matter is a relatively weak
805 oxygen sink and source of metabolic DIC.
806
807
808 5. Conclusion
809
810 The Truc Vert Beach is a high-energy beach affected by strong physical forcings (tides,
811 waves) that drive an active seawater recirculation cell within the intertidal sands. This tidally-
812 driven SGD is complemented by a terrestrial, fresh groundwater input from the coupled, upland
813 pine forest aquifer. Our results show that aerobic respiration processes are active in the seawater
814 circulation cell, particularly in spring and summer, leading to a substantial DIC flux to the
815 coastal ocean. Up-scaled over the 240 km-long Aquitaine coast, the carbon flux is estimated at
816 4400 tons of carbon per year to the Bay of Biscay coastal zone. The carbon isotopic signature
817 of the metabolic DIC, when coupled to pore water DIC and DOC concentrations, reveals that
818 aerobic respiration of marine organic matter trapped by the sand, as seawater brought up the
819 beach by tides and waves percolates through, is the main source of metabolic DIC within the
820 intertidal sands. Therefore, the efficient oxic degradation of marine organic carbon in high
821 energy beach aquifer prevents carbon storage within the sand and from being a source of DOC.
822 Analyses of pore waters sampled in the subterranean estuary of the supratidal beach
823 show that carbonate system parameters (TA, DIC, pH, pCO_2) do not behave conservatively
824 along the salinity gradient. Degassing of CO_2 to the atmosphere in the upper part of the beach
825 best explains the evolution of the measured parameters. Fresh groundwaters sampled on the
826 forest-side and beach-side of the bare foredune reveal that terrestrial groundwater is chemically
827 altered upstream of the beach. Unlike most STEs, the redox front at the Truc Vert Beach occurs
828 below the fore dune and does not coincide with the salinity gradient. Most of the CO_2 dissolved
829 in the forest groundwater that flows seaward though the connected aquifer, degasses in this
830 transition zone. We calculated that CO_2 evasion accounted for about 33% of the forest

831 groundwater DIC (8000 tons out of 24200 tons of carbon), leaving a residual DIC flux to the
832 coastal zone that was about four-fold higher than the metabolic DIC produced and released in
833 the beach recirculation cell. Extrapolating the C-CO_2 evasion to the 240 km of beach and
834 assuming an average width of 200 m for the fore dunes, the annual flux of C-CO_2 is estimated
835 at 1.6 mmol m^{-2} h^{-1}. This flux could possibly be measured by incubating a volume of air under
836 a chamber and following the evolution of the pCO_2 (1 m^3 of air contains about 16 mmol of
837 CO_2) for a few hours.
838 CO_2 degassing leads to a groundwater DIC:TA ratio <1, resulting in SGD buffering
839 receiving seawater against ocean acidification. This is another feature that distinguishes this
840 coastal environment from others where carbon fluxes through SGD have been studied and
841 shown to amplifying the impact of ocean acidification in the coastal zone (Robinson et al.,
842 2018). This study demonstrates that the foredune and the supratidal zone of coastal
843 environments, with typologies similar to the Truc Vert Beach, are not inert vectors of fluids
844 from the land to the coastal ocean, but significant sources of CO_2 to the atmosphere and, must
845 therefore be taken into consideration in SGD carbon budgets.
846
847 Acknowledgements
848
849 The authors wish to thank colleagues and students who helped us in the field and in the
850 laboratory (Bruno Deflandre, Sophie Ferreira, Sylvain Capo, Romain Naturel, Sylvain Rigaud,
851 Orianne Jolly, Jonathan Deborde) as well as K. Charlier for her precious help with the $\delta^{13}C$-
852 DIC measurements. This work was funded by the French national projects EC2CO-MOBISEA
853 and ESTAFET (CNRS-INSU), and PROTIDAL (ANR-06-BLANC-0040) and carried out in
854 the framework of the Cluster of Excellence COTE (ANR-10-LABX-45). A.M. thanks the
855 Institut France-Québec Maritime and IdEx (initiative d'excellence)-Bordeaux for financial
856 support during his visit and sabbatical leave at the Université de Bordeaux.
857
858 References
859
860 Abarca E., Karam H., Hemond H. F. and Harvey C. F. (2013) Transient groundwater dynamics
861 in a coastal aquifer: the effects of tides, the lunar cycle, and the beach profile. *Water Resour.*
862 *Res.* **49**, 2473-2488.
863 Abril G. and Frankignoulle M. (2001) Nitrogen-alkalinity interactions in the highly-polluted
864 Scheldt basin (Belgium). *Water Res.* **35**, 844-850.

865 Abril G., Bouillon S., Darchambeau F., Teodoru C.R., Marwick T.R., Tamooh F., Ochieng
866 Omengo F., Geeraert N., Deirmendjian L., Polsenaere P. and Borges A. V. (2015) Technical
867 note: Large overestimation of pCO_2 calculated from pH and alkalinity in acidic, organic-rich
868 freshwaters. *Biogeosciences* **12**, 67-78.
869 Andrews T. J. and Abel K. M. (1979) Photosynthetic carbon metabolism in seagrasses 14C-
870 labeling evidence for the C3 pathway. *Plant Physiol.* **63** 650-656, doi:10.1104/pp.63.4.650
871 Anschutz P., Charbonnier C., Deborde J., Deirmendjian L., Poirier D., Mouret A., Buquet D.
872 and Lecroart P. (2016) Terrestrial groundwater and nutrient discharge along the 240-km long
873 Aquitanian coast. *Mar. Chem.* **185**, 38-47.
874 Anschutz P., Charbonnier C. and Lecroart P. (2017) Nutrient and carbon fluxes along the sandy
875 beaches of the French Atlantic coast: recycling and groundwater discharge. *Goldschmidt*
876 *2017*, Paris. #10G(abstr.).
877 Anschutz P., Smith T., Mouret A., Deborde J., Bujan S., Poirier D. and Lecroart P. (2009) Tidal
878 sands as biogeochemical reactors. *Estuar. Coast. Shelf Sci* **84**, 84-90.
879 Atkins M. L., Santos I. R., Ruiz-Halpern S. and Maher D. T. (2013) Carbon dioxide dynamics
880 driven by groundwater discharge in a coastal floodplain creek. *J. Hydrol.* **493**, 30-42.
881 Avery G. B., Kieber R. J. and Taylor K. J. (2008) Nitrogen release from surface sand of a high
882 energy beach face along the Southeastern Coast of North Carolina, USA. *Biogeochemistry*
883 **89**, 357-365.
884 Avery G. B., Kieber R. J., Taylor K. J. and Dixon J. L. (2012) Dissolved organic carbon release
885 from surface sand of a high energy beach along the Southeastern Coast of North Carolina,
886 USA. *Mar. Chem.* **132**, 23-27.
887 Beck A. J., Tsukamoto Y., Tovar-Sanchez A., Huerta-Diaz M., Bokuniewicz H. J. and Sanudo-
888 Wilhelmy S. A. (2007) Importance of geochemical transformations in determining
889 submarine groundwater discharge-derived trace metal and nutrient fluxes. *Appl. Geochem.*
890 **22**, 477-490.
891 Beck M., Reckhardt A., Amelsberg J., Bartholomä A., Brumsack H.-J., Cypionka H., Dittmar
892 T., Engelen B., Greskowiak J., Hillebrand H., Holtappels M., Neuholz R., Köster J., Kuypers
893 M. M. M., Massmann G., Meier D., Niggemann J., Paffrath R., Pahnke K., Rovo S., Striebel
894 M., Vandieken V., Wehrmann A. and Zielinski O. (2017) The drivers of biogeochemistry in
895 beach ecosystems: A cross-shore transect from the dunes to the low-water line. *Mar. Chem.*
896 **190**, 35-50. doi.org/10.1016/j.marchem.2017.01.001.
897 Bokuniewicz H., Buddemeier R., Maxwell B., Smith C. (2003) The typological approach to
898 submarine groundwater discharge (SGD). *Biogeochemistry* **66**, 145-158.

899 Borges A. V. and Gypens N. (2010) Carbonate chemistry in the coastal zone responds more
900 strongly to eutrophication than to ocean acidification. *Limnol. Oceanogr.* **55**, 346-353.
901 doi:10.4319/lo.2010.55.1.0346
902 Bouillon S., Frankignoulle M., Dehairs F., Velimirov B., Eiler A., Abril G., Etcheber H. and
903 Borges A.V. (2003) Inorganic and organic carbon biogeochemistry in the Gautami Godavari
904 estuary (Andhra Pradesh, India) during pre-monsoon: the local impact of extensive
905 mangrove forests. *Global Biogeochem. Cycles* **17**(4), 1114, doi:10.1029/2002GB002026.
906 Bouillon S., Middleburg J. J., Dehairs F., Borges A.V., Abril G., Flindt M. R., Ulomi S. and
907 Kristensen E. (2007) Importance of intertidal sediment processes and porewater exchange
908 on the water column biogeochemistry in a pristine mangrove creek (Ras Dege, Tanzania).
909 *Biogeosciences* **4**, 311-322.
910 Bowen J.L., Kroeger K.D., Tomasky G., Pabich W.J., Cole M.L., Carmichael R.H. and Valiela
911 I. (2007) A review of land-sea coupling by groundwater discharge of nitrogen to New
912 England estuaries: mechanisms and effects. *Appl. Geochem.* **22**, 175-191.
913 Buquet D. (2017) Cycle des éléments biogènes dans les lacs côtiers en Gironde. Thesis, Univ.
914 Bordeaux. https://tel.archives-ouvertes.fr/tel-01617783
915 Buquet D., Sirieix C., Anschutz P., Malaurent P., Charbonnier C., Naessens F., Bujan S. and
916 Lecroart P. (2016) Shape of the shallow aquifer at the freshwater-seawater interface on a
917 high-energy sandy beach. *Estuar. Coast. Shelf Sci.* **179**, 79-89.
918 Burdige D. J. (2006) *Geochemistry of Marine Sediments*. Princeton University Press, Princeton.
919 Burnett W. C., Aggarwal P. K., Aureli A., Bokuniewicz H. J., Cable J. E., Charette M. A.,
920 Kontar E., Krupa S., Kulkarni K. M., Loveless A., Moore W. S., Oberdorfer J. A., Oliveira
921 J., Ozyurt N., Povinec P., Privitera A. M. G., Rajar R., Ramessur R. T., Scholten J., Stieglitz
922 T., Tanigushi M. and Turner J. V. (2006) Quantifying submarine groundwater discharge in
923 the coastal zone via multiple methods. *Sci. Tot. Environ.* **367**, 498-543.
924 Burnett W. C., Bokuniewicz H., Huettel M., Moore W. S. and Taniguchi M. (2003)
925 Groundwater and pore water inputs to the coastal zone. *Biogeochemistry* **66**, 3-33.
926 Cable J. E., Corbett D. and Walsh M. M. (2002) Phosphate uptake in coastal limestone aquifers:
927 a fresh look at wastewater management. *Limnol. Oceanogr. Bull.* **11**, 1-4.
928 Cai W. J., Wang Y., Krest J. and Moore, W. S. (2003) The geochemistry of dissolved inorganic
929 carbon in a surficial groundwater aquifer in North Inlet, South Carolina, and the carbon
930 fluxes to the coastal ocean. *Geochim. Cosmochim. Acta* **67**, 631-639.
931 Call M., Maher D. T., Santos I. R., Ruiz-Halpern S., Mangion P., Sanders C. J., Erler D. V. and
932 Eyre B. D. (2015) Spatial and temporal variability of carbon dioxide and methane fluxes

over semi-diurnal and spring-neap-spring timescales in a mangrove creek. *Geochim. Cosmochim. Acta* **150**, 211-225.

Carlson C. A. and Hansell D. A. (2014) DOM source, sinks, reactivity, and budgets. In *Biogeochemistry of Marine Dissolved Organic Matter* (eds. D. A. Hansell and C. A. Carlson), Academic Press, San Diego, CA, pp. 65–126.

Castelle B., Bonneton P., Dupuis H. and Sénéchal N. (2007) Double bar beach dynamics on the high-energy meso-macrotidal French Aquitanian Coast: a review. *Mar. Geol.* **245**, 141–159.

Castelle B., Marieu V., Bujan S., Ferreira S., Parisot J.P., Capo S., Sénéchal N. and Chouzenoux T. (2014) Equilibrium shoreline modelling of a high-energy meso– macrotidal multiple-barred beach. *Mar. Geol.* **347**, 85–94.

Cerling T. E., Solomon D. K., Quade J. and Bowman J. R. (1991) On the isotopic composition of carbon in soil carbon dioxide. *Geochim Cosmochim. Acta* **55**, 3403–3405.

Chaillou G., Lemay-Borduas F. and Couturier M. (2016) Transport and transformations of groundwater-borne carbon discharging through a sandy beach to a coastal ocean. *Can. Water Resour. J.*, doi.org/10.1080/07011784.2015.1111775

Charbonnier C., Anschutz P., Deflandre B., Bujan S. and Lecroart P. (2015) Measuring pore water oxygen of a high-energy beach using buried probes. *Estuar. Coast. Shelf Sci.* **179**, 66-78.

Charbonnier C., Anschutz P., Poirier D., Bujan S. and Lecroart P. (2013) Aerobic respiration in a high-energy sandy beach. *Mar. Chem.* **155**, 10-21.

Charette M. A., Henderson P. B., Breier C. F. and Liu Q. (2013) Submarine groundwater discharge in a river-dominated Florida estuary. *Mar. Chem.* **156**, 3-17.

Charette M. A. and Sholkovitz E. R. (2002) Oxidative precipitation of groundwater-derived ferrous iron in the subterranean estuary of a coastal bay. *Geophys. Res. Lett.* **29**, 85-1 - 85-4.

Charette M. A., Sholkovitz E. R. and Hansel C. M. (2005) Trace element cycling in a subterranean estuary: Part 1. Geochemistry of the permeable sediments. *Geochim. Cosmochim. Acta* **69**, 2095-2109.

Chen X., Zhang F., Lao Y., Wang X., Du J. and Santos I. R. (2018) Submarine groundwater discharge-derived carbon fluxes in mangroves: An important component of blue carbon budgets? *J. Geophys. Res: Oceans,* **123**, 6962-6979.

Cole J. J., Prairie Y. T., Caraco N. F., McDowell W. H., Tranvik L. J., Striegl R. G., Duarte M. C., Kortelainen P., Downing J. A., Middelburg J. J. and Melack J. (2007) Plumbing the global carbon cycle: integrating inland waters into the terrestrial carbon budget.

967 *Ecosystems* **10**, 172–185.
968 Cook P. L. M., Wenzhöfer F., Glud R. N., Janssen F. and Huettel M. (2007) Benthic solute
969 exchange and carbon mineralization in two shallow subtidal sandy sediments: Effect of
970 advective pore-water exchange. *Limnol. Oceanogr.* **52**, 1943-1963.
971 Couturier M., Nozais C. and Chaillou G. (2017) Microtidal subterranean estuaries as a source
972 of fresh terrestrial dissolved organic matter to the coastal ocean. *Mar. Chem.* **186**, 46-57.
973 Cyronak T., Santos I. R., McMahon A. and Eyre B. D. (2013) Carbon cycling hysteresis in
974 permeable carbonate sands over a diel cycle: Implications for ocean acidification. *Limnol.*
975 *Oceanogr.* **58**, 131-143.
976 de Weys J., Santos I. R. and Eyre B. D. (2011) Linking groundwater discharge to severe
977 estuarine acidification during a flood in a modified wetland. *Environ. Sci. Technol.* **45**, 3310-
978 3316. doi.org/10.1021/es104071r.
979 Deirmendjian L. and Abril G. (2018) Carbon dioxide degassing at the groundwater-stream-
980 atmosphere interface: isotopic equilibration and hydrological mass balance in a sandy
981 watershed. *J. Hydrol.* **558**, 129-143.
982 Dickson A. G. and Millero F. J. (1987) A comparison of the equilibrium constants for the
983 dissociation of carbonic acid in seawater media. Deep Sea Res. Part A **34**, 1733–1743.
984 Dorsett A., Cherrier A. J., Martin J. B. and Cable J.E. (2011) Assessing hydrologic and
985 biogeochemical controls on pore-water dissolved inorganic carbon cycling in a subterranean
986 estuary: A ^{14}C and ^{13}C mass balance approach. *Mar. Chem.* **127**, 76-89.
987 Dubois S., Savoye N., Grémare A., Plus M., Charlier K., Beltoise A. and Blanchet H. (2012)
988 Origin and composition of sediment organic matter in a coastal semi-enclosed ecosystem:
989 An elemental and isotopic study at the ecosystem space scale. *J. Mar. Syst.* **94**, 64–73.
990 Dugan J. E., Hubbard D. M., Page H. M. and Schimel J. P. (2011) Marine macrophyte wrack
991 inputs and dissolved nutrients in beach sands. *Estuar. Coasts* **34**, 839-850.
992 Ehleringer J. R., Rundel P. W. and Nagy K. A. (1986) Stable Isotopes in Physiological Ecology
993 and Food Web Research. Trends Ecol. Evol. **1**, 42-45.
994 Faber P. A., Evrard V., Woodland R. J., Cartwright I. C. and Cook P. L. M. (2014) Pore-water
995 exchange driven by tidal pumping causes alkalinity export in two intertidal inlets. *Limnol.*
996 *Oceanogr.* **59**, 1749-1763.
997 Frankignoulle M. and Borges A. V. (2001) Direct and indirect pCO_2 measurements in a wide
998 range of pCO_2 and salinity values. *Aquat. Geochem.* **7**, 267-273.

999 Fry B. (2002) Conservative mixing of stable isotopes across estuarine salinity gradients: A
1000 conceptual framework for monitoring watershed influences on downstream fisheries
1001 production. *Estuaries* **25**, 264–271.
1002 Gagan M. K., Ayliffe L. K., Opdyke B. N., Hopley D., Scott-Gagan H. and Cowley J. (2002)
1003 Coral oxygen isotope evidence for recent groundwater fluxes to the Australian Great Barrier
1004 Reef. *Geophys. Res. Lett.* **29**, 43-1 to 43-4.
1005 Gattuso, J. P., and Hansson, L. (2011). Ocean acidification: background and history. In *Ocean*
1006 *Acidification* (eds. J. P. Gattuso and L. Hansson).Oxford University Press, New York, pp.
1007 1-20.
1008 Gattuso J. P., Frankignoulle M. and Wollast R. (1998) Carbon and carbonate metabolism in
1009 coastal aquatic ecosystems. *Annu. Rev. Ecol. System.* **29**, 405-434.
1010 Gillikin D. P. and Bouillon S. (2007) Determination of $\delta^{18}O$ of water and $\delta^{13}C$ of dissolved
1011 inorganic carbon using a simple modification of an elemental analyzer-isotope ratio mass
1012 spectrometer EA-IRMS: an evaluation. *Rapid Com. Mass Spectrometry* **21**, 1475-1478.
1013 Gleeson J., Santos I. R., Maher D. T. and Golsby-Smith L. (2013) Groundwater-surface water
1014 exchange in a mangrove tidal creek: Evidence from natural geochemical tracers and
1015 implications for nutrient budgets. *Mar. Chem.* **156**, 27-37.
1016 Goñi M. A., and Gardner L.R. (2003) Seasonal dynamics in dissolved organic carbon
1017 concentrations in a coastal-water-table aquifer at the forest-marsh interface. *Aquat.*
1018 *Geochem.* **9**, 209-232.
1019 Goodridge B. M. (2018) The influence of submarine groundwater discharge on nearshore
1020 marine dissolved organic carbon reactivity, concentration dynamics, and offshore export.
1021 *Geochim. Cosmochim. Acta* **241**, 108-119.
1022 Gran G. (1952) Determination of the equivalence point in potentiometric titrations, part II.
1023 *Analyst* **77**, 661-671.
1024 Hanson P. J., Edwards N. T., Garten C. T., and Andrews J. A. (2000). Separating root and soil
1025 microbial contributions to soil respiration: A review of methods and observations.
1026 *Biogeochemistry* **48**(1), 115-146. doi:10.1023/A:1006244819642
1027 Huettel M. and Rush A. (2000) Transport and degradation of phytoplankton in permeable
1028 sediments. *Limnol. Oceanogr.* **45**, 534-549.
1029 Jeffrey L. C., Maher D. T., Santos I. R., McMahon A., Tait D. R. (2016) Groundwater, acid and
1030 carbon dioxide dynamics along a coastal wetland, lake and estuary continuum, *Estuar.*
1031 *Coasts* **39**, 1325-1344. doi.org/10.1007/s12237-016-0099-8.

1032 Keeling C. (1958) The concentration and isotopic abundances of atmospheric carbon dioxide
1033 in rural areas. *Geochim. Cosmochim. Acta* **13**, 322-334.
1034 Kim G., Ryu J. W., Yang H. S. and Yun S. T. (2005) Submarine groundwater discharge (SGD)
1035 into the Yellow Sea revealed by Ra-228 and Ra-226 isotopes: implications for global silicate
1036 fluxes. *Earth Planet. Sci. Lett.* **237**, 156-166.
1037 Kim T. H., Waska H., Kwon E., Suryaputra I. G. N. and Kim G. (2012) Production, degradation,
1038 and flux of dissolved organic matter in the subterranean estuary of a large tidal flat. *Mar.*
1039 *Chem.* **142-144**, 1-10.
1040 Komada T., Polly J. A. and Johnson L. (2012) Transformations of carbon in anoxic marine
1041 sediments: Implications from $\Delta^{14}C$ and $\delta^{13}C$ signatures. *Limnol. Oceanogr.* **57**, 567-581.
1042 Koné Y. M. and Borges A. (2008) Dissolved inorganic carbon dynamics in the waters
1043 surrounding forested mangroves of the Ca Mau Province (Vietnam). *Estuar. Coast. Shelf*
1044 *Sci.* **77**, 409-421.
1045 Kristensen E. and Hansen K. (1995) Decay of plant detritus in organic-poor marine sediment:
1046 Production rates and stoichiometry of dissolved C and N compounds. *J. Mar. Res.* **53**, 675-
1047 702.
1048 Lee J. and Kim G. (2015) Dependence of coastal water pH increases on submarine groundwater
1049 discharge off a volcanic island. *Estuar. Coast. Shelf Sci.* **163**, 15-21.
1050 Lee J. M. and Kim G. (2007) Estimating submarine discharge of fresh groundwater from a
1051 volcanic island using a freshwater budget of the coastal water column. *Geophys. Res. Lett.*
1052 **34**, L11611.
1053 Lee Y. W., Kim G., Lim W. A. and Hwang D. W. (2010) A relationship between submarine
1054 groundwater-borne nutrients traced by Ra isotopes and the intensity of dinoflagellate red-
1055 tides occurring in the southern sea of Korea. *Limnol. Oceanogr.* **55**, 1-10.
1056 Legigan P. (1979) L'élaboration de la formation du Sable des Landes, dépôt résiduel de
1057 l'environnement sédimentaire pliocène-pléistocène centre aquitain. Thesis, Univ. Bordeaux.
1058 Liu Q., Charette M. A., Breier C. F., Henderson P. B., McCorkle D. C., Martin W. and Dai M.
1059 (2017) Carbonate system biogeochemistry in a subterranean estuary – Waquoit Bay, USA.
1060 *Geochim. Cosmochim. Acta* **203**, 422-439.
1061 Liu Q., Charette M. A., Henderson P. B., McCorkle D. C., Martin W. and Dai M. (2014) Effect
1062 of submarine groundwater discharge on the coastal ocean inorganic carbon cycle. *Limnol.*
1063 *Oceanogr.* **59**, 1529-1554.

1064 Liu Q., Dai M., Chen W., Huh A., Wang G., Li Q. and Charette M. A. (2012) How significant
1065 is submarine groundwater discharge and its associated dissolved inorganic carbon in a river-
1066 dominated shelf system ? *Biogeosciences* **9**, 1777-1795.
1067 Lyman J. (1975) Buffer mechanism of seawater. PhD thesis, Univ. California, Los Angeles.
1068 Macklin P. A., Maher D. T. and Santos I. R. (2014) Estuarine canal estate water : hotspots of
1069 CO_2 outgassing driven by enhanced groundwater discharge? *Mar. Chem.* **167**, 82-92.
1070 Maher D. T., Santos I. R., Golsby-Smith L., Gleeson J. and Eyre B. D. (2013) Groundwater-
1071 derived dissolved inorganic and organic carbon exports from a mangrove tidal creek: The
1072 missing mangrove carbon sink ? *Limnol. Oceanogr.* **58**, 475-488.
1073 Mehrbach C., Culberson C. H., Hawley J. E. and Pytkowicz R. N. (1973) Measurement of the
1074 apparent dissociation constants of carbonic acid in sea water at atmospheric pressure.
1075 *Limnol. Oceanogr.* **18**, 897-907.
1076 Michel D. and Howa H. (1999) Short-term morphodynamic response of a ridge and runnel
1077 system on a mesotidal sandy beach. *J. Coast. Res.* **15**, 428–437.
1078 Miyajima T., Tsuboi Y., Tanaka Y. and Koike I. (2009) Export of inorganic carbon from two
1079 Southeast Asian mangrove forests to adjacent estuaries as estimated by the stable isotope
1080 composition of dissolved inorganic carbon. *J. Geophys. Res.* **114**, G01024.
1081 Miyajima T., Yamada Y., Hanba Y. T., Yoshii K., Koitabashi T. and Wada E. (1995)
1082 Determining the stable isotope ratio of total dissolved inorganic carbon in lake water by
1083 GC/C/IRMS. *Limnol. Oceanogr.* **40**, 994-1000.
1084 Mook W. G. (2000) Environmental isotopes in the hydrological cycle - Principles and
1085 applications. Technic. Doc. Hydrol. **39**, UNESCO, Paris.
1086 Mook W. G., Bommerson J. C., and Staverman W. H. (1974) Carbon isotope fractionation
1087 between dissolved bicarbonate and gaseous carbon dioxide. *Earth Planet. Sci. Lett.* **22**(2),
1088 169-176. doi:10.1016/0012-821X(74)90078-8
1089 Moore W. S. (1999) The subterranean estuary: a reaction zone of groundwater and seawater.
1090 *Mar. Chem.* **65**, 111-125.
1091 Moore W. S. (2006) The role of submarine groundwater discharge in coastal biogeochemistry.
1092 J. Geochem. Explor. **88**, 389-393.
1093 Moore W. S., Beck M., Riedel T., Rutgers van der Loeff M., Dellwig O., Shaw T. J., Schnetger
1094 B. and Brumsack H. J. (2011) Radium-based pore water fluxes of silica, alkalinity,
1095 manganese, DOC, and uranium: a decade of studies in the German Wadden Sea. *Geochim.*
1096 *Cosmochim. Acta* **75**, 6535-6555.

1097 Moore W. S., Blanton J. O. and Joye S. B. (2006) Estimates of flushing times, submarine
1098 groundwater discharge, and nutrient fluxes to Okatee Estuary, South Carolina. *J. Geophys.*
1099 *Res.: Oceans* **111**, 1978-2012.
1100 Mouret A., Charbonnier C., Lecroart P., Metzger E., Howa H., Deflandre B., Deirmendjian L.,
1101 Anschutz P. (2020) Biogeochemistry in an intertidal pocket beach. *Estuar. Coast. Shelf Sci.*
1102 **243**, 106920. 10.1016/j.ecss.2020.106920
1103 Orr J. C., Fabry V. J., Aumont O., Bopp L., Doney S. C., Feely R. A., Gnanadesikan A., Gruber
1104 N., Ishida A., Joos F., Key R. M., Lindsay K., Maier-Reimer E., Matear R., Monfray P.,
1105 Mouchet A., Najjar R. G., Plattner G. K., Rodgers K. B., Sabine C. L., Sarmiento J. L.,
1106 Schlitzer R., Slater R. D., Totterdell I. J., Weiring M. F., Yamanaka Y. and Yool A. (2005)
1107 Anthropogenic ocean acidification over the twenty-first century and its impact on calcifying
1108 organisms. *Nature*, **437**, 681–686.
1109 Pain A. J., Martin J. B. and Young C. R. (2019) Sources and sinks of CO2 and CH4 in
1110 siliciclastic subterranean estuaries. *Limnol. Oceanogr.* **64**, 1500-1514.
1111 doi:10.1002/lno.11131
1112 Pataki D. E., Bowling D. R. and Ehleringer J. R. (2003) Seasonal cycle of carbon dioxide and
1113 its isotopic composition in an urban atmosphere: Anthropogenic and biogenic effects. *J.*
1114 *Geophys. Res.: Atmospheres* **108**, 4735.
1115 Perkins A. K., Santos I. R., Sadat-Noori M., Gatland J. R. and Maher D. T. (2015) Groundwater
1116 seepage as a driver of CO_2 evasion in a coastal lake (Lake Ainsworth, NSW, Australia).
1117 *Environm. Earth Sci*. **74**, 779–792.
1118 Polsenaere P. and Abril G. (2012) Modelling CO_2 degassing from small acidic rivers using
1119 water pCO_2, DIC and δ^{13}C-DIC data. *Geochim. Cosmochim. Acta* **91**, 220–239.
1120 Polsenaere P., Savoye N., Etcheber H., Canton M., Poirier D., Bouillon S. and Abril G. (2013)
1121 Export and degassing of terrestrial carbon through watercourses draining a temperate
1122 podzolized catchment. *Aquat. Sci.* **75**, 299-319.
1123 Porubsky W. P., Weston N. B., Moore W. S., Ruppel C. and Joye S. B. (2014) Dynamics of
1124 submarine groundwater discharge and associated fluxes of dissolved nutrients, carbon, and
1125 trace gases to the coastal zone (Okatee River estuary, South Carolina). *Geochim.*
1126 *Cosmochim. Acta* **131**, 81-97.
1127 Rauch M., Denis L. and Dauvin J.C. (2008) The effects of *Phaeocystis globosa* bloom on the
1128 dynamics of the mineralization processes in intertidal permeable sediment in the eastern
1129 English Channel (Wimereux, France). *Mar. Pollut. Bull.* **56**, 1284-1293.

Reckhardt A., Beck M., Seidel M., Riedel T., Wehrmann A., Bartholomä A., Schnetger B., Dittmar T. and Brumsack H. J. (2015) Carbon, nutrient and trace metal cycling in sandy sediments: A comparison of high-energy beaches and backbarrier tidal flats. *Estuar. Coast. Shelf Sci.* **159**, 1-14.

Robinson C., Li L. and Barry D.A. (2007) Effect of tidal forcing on a subterranean estuary. *Adv. Wat. Resour.* **30**, 851-865.

Robinson C. E., Xin P., Santos I. R., Charette M. A., Li L. and Barry D. A. (2018) Groundwater dynamics in subterranean estuaries of coastal unconfined aquifers : Controls on submarine groundwater discharge and chemical inputs to the ocean. *Adv. Water Resour.* **115**, 315–331. doi.org/10.1016/j.advwatres.2017.10.041.

Rocha C. (2008) Sandy sediments as active biogeochemical reactors: compound cycling in the fast lane. *Aquat. Microb. Ecol.* **53**, 119-127.

Sadat-Noori M., Maher D. T. and Santos I. R. (2016) Groundwater Discharge as a Source of Dissolved Carbon and Greenhouse Gases in a Subtropical Estuary. *Estuar. Coasts* **39**, 639-656.

Santos I. R., Beck M., Brumsack H. J., Maher D. T., Dittmar T., Waska H. and Schnetger B. (2015) Porewater exchange as a driver of carbon dynamics across a terrestrial-marine transect: insights from coupled 222Rn and pCO_2 observations in the German Wadden Sea. *Mar. Chem.* **171**, 10-20.

Santos I. R., Bryan K. R., Pilditch C. A. and Tait D. R. (2014) Influence of porewater exchange on nutrient dynamics in two New Zealand estuarine intertidal flats. *Mar. Chem.* **167**, 57-70.

Santos I. R., Burnett W., Dittmar T., Suryaputra I. and Chanton J. (2009) Tidal pumping drives nutrient and dissolved organic matter dynamics in a Gulf of Mexico subterranean estuary. *Geochim. Cosmochim. Acta* **73**, 1325-1339.

Santos I. R., Cook P. L. M., Rogers L., De Weys J. and Eyre B. D. (2012a). The "salt wedge pump": convection-driven-pore-water exchange as a source of dissolved organic and inorganic carbon and nitrogen to an estuary. *Limnol. Oceanogr.* **57**, 1415-1426.

Santos I. R., Eyre B.D. and Huettel M. (2012b) The driving forces of porewater and groundwater flow in permeable coastal sediments: a review. *Estuar*. *Coast*. *Shelf Sci*. **98**, 1–15.

Savoy L., Surbeck H. and Hunkeler D. (2011) Radon and CO_2 as natural tracers to investigate the recharge dynamics of karst aquifers. *J. Hydrol.* **406**, 148-157.

Sharp J. H. (1993) The dissolved organic carbon controversy: an update. *Oceanography* **6**, 45-50.

1164 Slomp C. P. and Van Cappellen P. (2004) Nutrients inputs to the coastal ocean through
1165 submarine groundwater discharge: controls and potential impact. *J. Hydrol.* **295**, 64-86.
1166 Spiteri C., Slomp C. P., Charette M. A., Tuncay K. and Meile C. (2008) Flow and nutrient
1167 dynamics in a subterranean estuary (Waquoit Bay, MA, USA): field data and reactive
1168 transport modeling. *Geochim. Cosmochim. Acta* **72**, 3398-3412.
1169 Stewart B. T., Santos I. R., Tait D. R., Macklin P. A. and Maher D. T. (2015) Submarine
1170 groundwater discharge and associated fluxes of alkalinity and dissolved carbon into Moreton
1171 Bay (Australia) estimated via radium isotopes. *Mar. Chem.* **174**, 1-12.
1172 Stumm W. and Morgan J. (1996) *Aquatic Chemistry* (3rd edition). J. Wiley and Sons editions,
1173 New York.
1174 Swarzenski P. W., Orem W. H., McPherson B. F., Baskaran M. and Wan Y. (2006)
1175 Biogeochemical transport in the Loxahatchee River estuary, Florida: The role of submarine
1176 groundwater discharge. *Mar. Chem.* **101**, 248-265.
1177 Takahashi T., Olafsson J., Goddard J., Chipman D. W. and Sutherland S. C. (1993) Seasonal
1178 variation of CO2 and nutrients in the high-latitude surface oceans: a comparative study.
1179 *Global Biogeochem. Cycles* **7**, 843–878.
1180 Uppström L. R. (1974) The boron/chlorinity ratio of deep-sea water from the Pacific Ocean.
1181 *Deep Sea Res.* **21**, 161-162.
1182 Wang G., Wang Z., Zhai W., Moore W. S., Li Q., Yan X., Qi D. and Jiang Y. (2015) Net
1183 subterranean estuarine export fluxes of dissolved inorganic C, N, P, Si, and total alkalinity
1184 into the Jiulong River estuary, China. *Geochim. Cosmochim. Acta* **149**, 103-114.
1185 Wang S. L., Chen C. T. A., Huang T. H., Tseng H. C., Lui H. K., Peng T. R., Kandasamy S.,
1186 Zhang J., Yang L., Gao X., Lou J. Y., Kuo F. W., Chen X. G., Ye Y. and Lin Y. L. (2018)
1187 Submarine Groundwater Discharge helps making nearshore waters heterotrophic. *Nature*,
1188 Scientific Reports **8**, 11650.
1189 Weinstein Y., Burnett W. C., Swarzenski P. W., Shalem Y., Yechieli Y., Herut B. (2007) Role
1190 of aquifer heterogeneity in fresh groundwater discharge and seawater recycling: An example
1191 from the Carmel coast, Israel. *J. Geophys. Res.: Oceans* **112**, 1978-2002.
1192 Weiss R. F. (1974) Carbon dioxide in water and seawater: the solubility of a non-ideal gas.
1193 *Mar. Chem.* **2** 203-215.
1194 Windom H. and Niencheski F. (2003) Biogeochemical processes in a freshwater-seawater
1195 mixing zone in permeable sediments along the coast of Southern Brazil. *Mar. Chem.* **83**,
1196 121-130.
1197

Figure 1: Location of Truc Vert Beach, on the SW coast of France.

Figure 2: Schematic W-E cross-section of the beach-dune system and the different waters sampled (1 – seawater; 2 – beach pore waters; 3 –piezometers in the supratidal zone; 4 – forest wells), with a conceptual diagram of the subterranean estuary of the Truc Vert Beach. Grey arrows represent major nearshore flow processes: (A) seawater circulation induced by waves and tides, called "intertidal saline plume", and (B) parcels of brackish water discharge, as revealed by geophysical data (Buquet et al., 2016).

Figure 3: Evolution with time of DIC, O_2, DOC, pCO_2 and δ^{13}C-DIC in interstitial waters from tidally-driven recirculation of seawater in Truc Vert Beach. The pore water values are derived from samples with salinity close to that of seawater. Samples mixed with freshwater were discarded. The values for the lower beach come from the most O_2 depleted sample of each cross-shore profile; the values for the upper beach come from the sample taken closest to the dune of each cross-shore profile.

Figure 4: (A) Altitude at the top of the water table and location of probes and the three supratidal piezometers. Practical salinity (S_P) and δ^{13}C-DIC (grey characters) are indicated for each piezometer for both the neap and spring tides in February-March 2013. (B) DIC, pCO_2, oxygen saturation and salinity values of the pore waters at the three supratidal piezometers during a spring-neap tidal cycle in February-March 2013 and September-October 2013. Note that there is no data at PZ1 for a few days during the neap tide because of the emersion of the instrument.

Figure 5: Conceptual diagram showing an overview the the end-members and processes affecting carbon in fresh groundwaters from the forest aquifer to the supratidal aquifer, and in the tidally-driven seawater circulation cell. For the latter, annual averages are shown. The seasonal evolution of the parameters is shown in Figure S2 of the supplementary material. Water discharge values are in m^3 per meter longshore per tide for the Truc Vert Beach site.

Figure 6: Assessment of the behaviour of DIC along the subterranean estuary of the Truc Vert Beach: (A) DIC concentrations versus practical salinity; (B) δ^{13}C-DIC versus practical salinity; (C) pCO_2 versus practical salinity; (D) δ^{13}C-DIC versus DIC concentrations. The grey lines denote the expected DIC (A) and δ^{13}C-DIC (B) values for conservative mixing between supratidal beach freshwaters and seawater. The black lines denote the expected DIC (A) and δ^{13}C-DIC (B) values for conservative mixing between continental freshwaters (forest wells) and seawater.

Figure 7: The δ^{13}C-DIC of pore waters from the lower Truc Vert Beach: (A) δ^{13}C-DIC versus consumed oxygen in saline ($S_P > 34.5$; light grey diamonds) and brackish ($S_P < 34.5$; dark grey diamonds) water; (B) δ^{13}C-DIC versus practical salinity and definition of four groups of pore waters depending on the mixing behaviour between supratidal beach fresh groundwaters and seawater. TML = theoretical mixing line; (C) Keeling plot of DIC-enriched, saline ($S_P > 34.5$) pore waters with low δ^{13}C-DIC for each of the four seasons in 2011; (D) Keeling plot of DIC-enriched brackish pore waters characterized by high δ^{13}C-DIC; (E) Keeling plot of brackish pore waters placed close to the theoretical mixing line and little affected by respiration processes ($O_2 > 85\%$); (F) Keeling plot of DIC-enriched brackish pore waters with low δ^{13}C-DIC values and affected by respiration processes (consumed $O_2 > 100$ μM).

1248 Table 1: pH, DOC and DIC concentrations, pCO_2 and $\delta^{13}C$-DIC values in continental
1249 groundwater collected in forest wells above the Truc Vert Beach in 2013 - 2014.
1250

Name of well	Sampling date	pH	DOC (μM)	DIC (μM)	pCO_2 (ppm)	$\delta^{13}C$-DIC (‰)
ONF	Feb. 2013	7.38	-	6040	11480	-16.7
DFCI 1	March 2013	7.30	1180	4650	10730	-14.3
	Sept. 2013	7.53	1060	3360	5170	-13.9
	Jan. 2014	7.01	2220	5470	23350	-16.6
DFCI 2	Sept. 2013	6.27	3170	6180	82640	-18.5
	Jan. 2014	6.47	5800	2120	21000	-22.5
DFCI 3	March 2013	7.01	2040	5210	20220	-16.4
	Sept. 2013	7.14	1150	4860	16400	-15.9
	Jan. 2014	7.03	2320	5280	21940	-16.5
DFCI 4	Jan. 2014	6.96	1820	4430	20840	-17.1
DFCI 5	Jan. 2014	6.96	1860	4680	22170	-17.2
DFCI 6	Jan. 2014	7.43	1810	4060	7840	-17.1

1251
1252
1253

Table 2: Average (± standard deviation) values of practical salinity (S_P), dissolved oxygen saturation, Fe(II), NH_4^+, pH, TA, DIC, pCO_2 and $\delta^{13}C$-DIC in continental, fresh groundwaters (forest wells), pore waters in the salinity gradient of the STE (supratidal beach piezometers), brackish pore waters of the lower beach and surface seawater.

	Continental freshwaters	Upper beach piezometers			Brackish PW of the lower beach	Seawater
		$S_P < 1$	$1 < S_P < 2$	$2 < S_P < 25$		
	(n = 12)	(n = 36)	(n = 10)	(n = 9)	(n = 28)	(n = 37)
S_P	0.0 ± 0.0	0.6 ± 0.1	1.2 ± 0.3	10.2 ± 6.1	31.4 ± 1.6	35.1 ± 0.4
O_2 (%)	0 ± 0	40 ± 32	37 ± 20	76 ± 14	51 ± 24	97 ± 6
Fe(II) (µM)*	59 ± 30	0.1 ± 0.2	0.2 ± 0.2	0.1 ± 0.2	-	< DL
NH_4^+ (µM)*	17 ± 18	0.5 ± 1.4	0.3 ± 0.3	0.2 ± 0.4	0.2 ± 0.4	< DL
pH	7.06 ± 0.37	7.94 ± 0.19	8.31 ± 0.20	8.20 ± 0.13	7.97 ± 0.12	8.20 ± 0.05
TA (µM)	3583 ± 1312	3441 ± 346	3171 ± 309	2903 ± 238	2455 ± 132	2311 ± 110
DIC (µM)	4700 ± 1130	3500 ± 380	3150 ± 330	2870 ± 260	2300 ± 160	2070 ± 100
pCO_2 (ppm)	16470 ± 6510**	2340 ± 1070	770 ± 380	810 ± 310	770 ± 250	400 ± 60
$\delta^{13}C$-DIC (‰)	-16.9 ± 2.2	-12.1 ± 0.1***	-9.9***	-5.2***	-1.3 ± 1.0	+0.4 ± 0.5

**after Anschutz et al. (2016)*

***n = 11, as an overestimated value was deleted for well DFCI2*

****n = 5 for $S_P < 1$; n = 1 for $1 < S_P < 2$; n =2 for $2 < S_P < 25$*

Table 3: Benthic DIC fluxes in permeable sediments with various fresh, groundwater inputs. Modified from Sadat-Noori et al. (2016).

Location	System description	DIC flux ($mmolC.m^{-2}.d^{-1}$)	Reference
Systems with high fresh groundwater input			
Waquoit Bay, USA	Semi-enclosed bay	1151	Liu et al., 2017
Hat Head, Australia	Groundwater discharge in a subtropical estuary	687	Sadat-Noori et al., 2016
Jiulong River estuary, China	Groundwater discharge in a river estuary	121-897	Wang et al., 2015
Moreton Bay, Australia	Embayment	153	Stewart et al., 2015
Okatee Estuary, USA	Salt marsh/estuary	1079	Porubsky et al., 2014
North Creek, Australia	Freshwater tidal creek	1810	Atkins et al., 2013
Moreton Bay, Australia	Mangrove tidal creek	183-342	Maher et al., 2013
Yarra River, Australia	Salt wedge estuary	349	Santos et al., 2012
Indian River Lagoon, USA	Coastal lagoon	120-340	Dorsett et al., 2011
Okatee Estuary, USA	Salt marsh/estuary	1963	Moore et al., 2006
North Inlet, USA	Salt marsh/estuary	171	Cai et al., 2003
Watson Inlet, Australia	Intertidal inlet with freshwater input	440	Faber et al., 2014
Systems with no or low freshwater input			
Heron Island, Australia	Permeable carbonate sediments	1.6-18.8	Cyronak et al., 2013
Chinaman Inlet, Western Port, Australia	Intertidal inlet without freshwater input	120	Faber et al., 2014
Southwest Florida Shelf, USA	Estuarine SGD to a subtropical carbonate platform	28-45	Liu et al., 2014
South China Sea	River-dominated continental shelf	16-36	Liu et al., 2012
Sylt Island, Germany	Advective saline pore water exchange in nearshore permeable sediments	31-120	Cook et al. 2007
Hel Peninsula, Poland	Advective saline pore water exchange in nearshore permeable sediments	5-42	Cook et al., 2007
Truc Vert Beach, SW France	*seawater recirculation + fresh groundwater*	*27* *130*	*This study*

Table 4: Practical salinity, DIC concentration and δ^{13}C-DIC measured in brackish, DIC-enriched and O_2-depleted pore waters of the lower beach. The theoretical DIC and δ^{13}C-DIC values are derived from conservative mixing between upper-beach fresh, groundwater and seawater. For each sample, the $\delta^{13}C_{added}$ is calculated using equation (6) from Bouillon et al. (2003).

Sample ID	Measured values			Theoretical values		$\delta^{13}C_{added}$ (‰)
	Salinity	DIC (µM)	δ^{13}C-DIC (‰)	DIC (µM)	δ^{13}C-DIC (‰)	
#1	30.5	2340	-2.28	2240	-2.17	-4.8
#2	31.2	2510	-2.70	2209	-1.80	-9.3
#3	32.4	2330	-1.52	2157	-1.15	-6.4
#4	32.8	2540	-3.36	2140	-0.92	-16.3
#5	33.1	2530	-2.58	2122	-0.75	-12.0
#6	33.5	2340	-1.76	2109	-0.52	-13.0
#7	33.5	2510	-3.06	2109	-0.52	-16.3
#8	33.6	2360	-1.79	2105	-0.46	-12.6
#9	34.1	2400	-2.70	2083	-0.17	-19.0

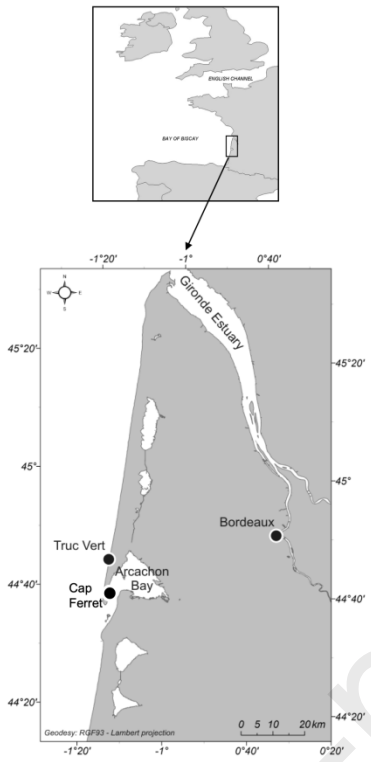

Figure 1: Location of Truc Vert Beach, on the SW coast of France.

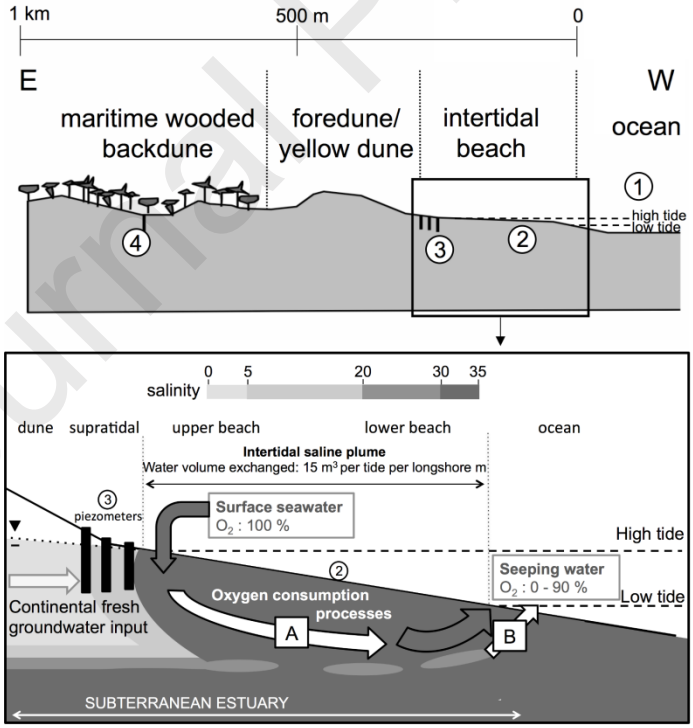

Figure 2: Schematic W-E cross-section of the beach-dune system and the different waters sampled (1 – seawater; 2 – beach pore waters; 3 –piezometers in the supratidal zone; 4 – forest wells), with a conceptual diagram of the subterranean estuary of the Truc Vert Beach. Grey arrows represent major nearshore flow processes: (A) seawater circulation induced by waves and tides, called "intertidal saline plume", and (B) parcels of brackish water discharge, as revealed by geophysical data (Buquet et al., 2016).

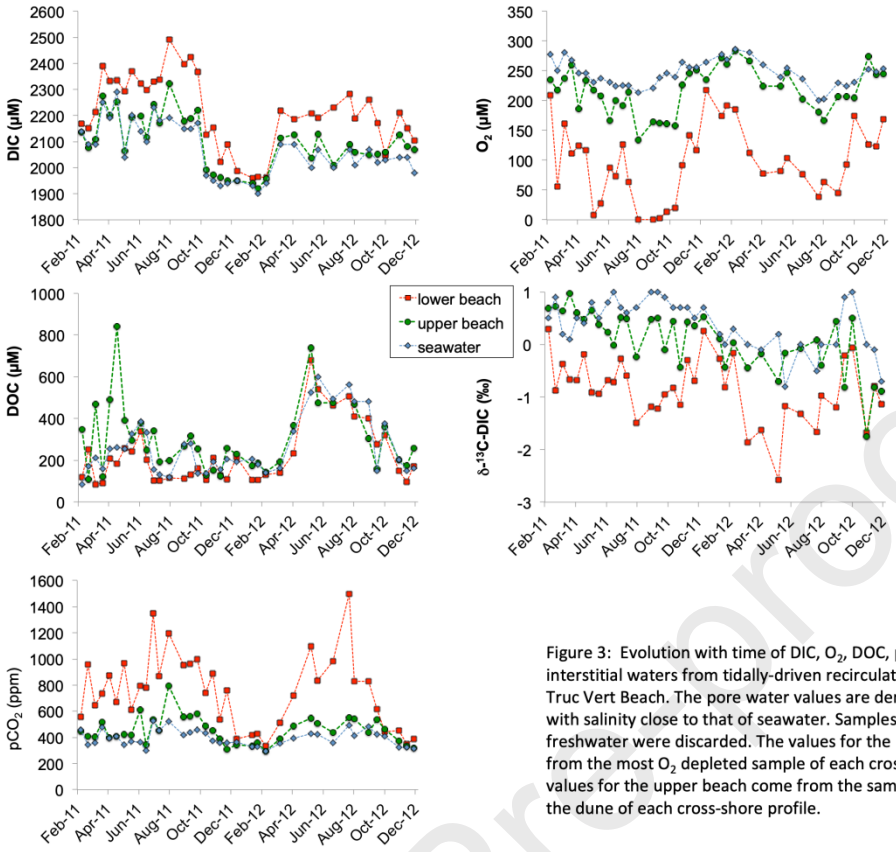

Figure 3: Evolution with time of DIC, O_2, DOC, pCO_2 and δ^{13}C-DIC in interstitial waters from tidally-driven recirculation of seawater in Truc Vert Beach. The pore water values are derived from samples with salinity close to that of seawater. Samples mixed with freshwater were discarded. The values for the lower beach come from the most O_2 depleted sample of each cross-shore profile; the values for the upper beach come from the sample taken closest to the dune of each cross-shore profile.

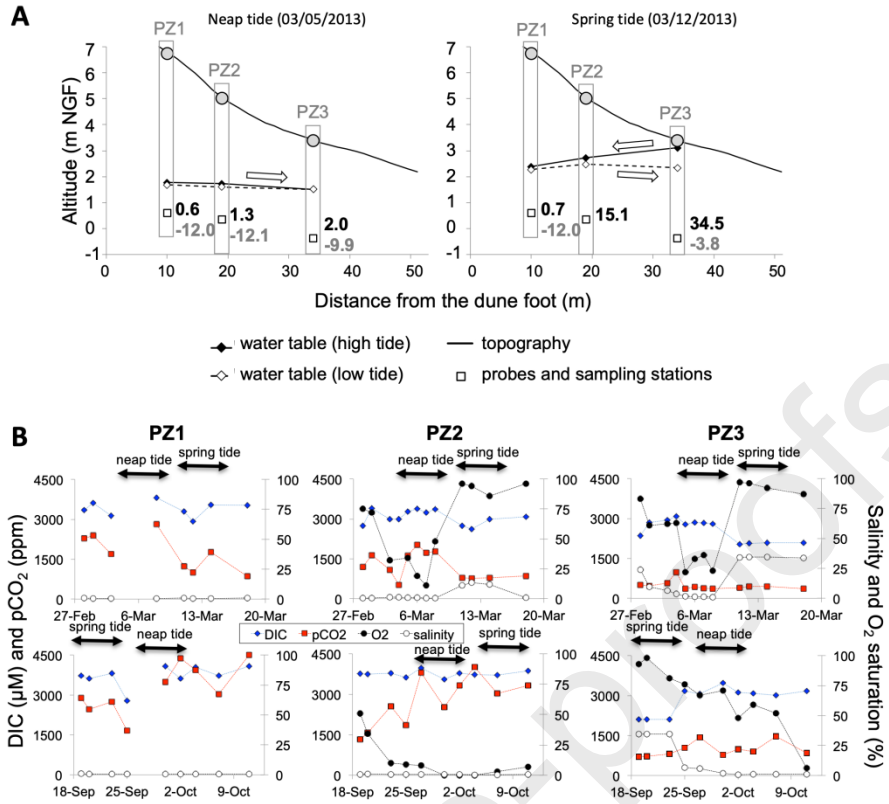

Figure 4: (A) Altitude at the top of the water table and location of probes and the three supratidal piezometers. Practical salinity (S_P) and δ^{13}C-DIC (grey characters) are indicated for each piezometer for both the neap and spring tides in February-March 2013. (B) DIC, pCO_2, oxygen saturation and salinity values of the pore waters at the three supratidal piezometers during a spring-neap tidal cycle in February-March 2013 and September-October 2013. Note that there is no data at PZ1 for a few days during the neap tide because of the emersion of the instrument.

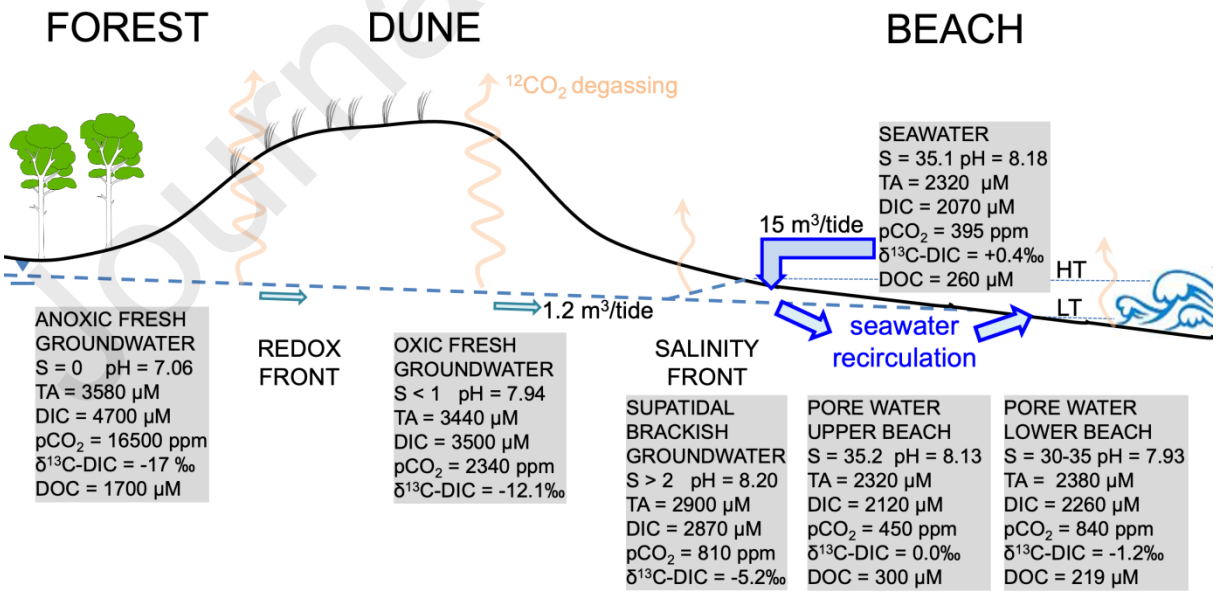

Figure 5: Conceptual diagram showing an overview the the end-members and processes affecting carbon in fresh groundwaters from the forest aquifer to the supratidal aquifer, and in the tidally-driven seawater circulation cell. For the latter, annual averages are shown. The seasonal evolution of the parameters is shown in Figure S2 of the supplementary material. Water discharge values are in m^3 per meter longshore per tide for the Truc Vert Beach site.

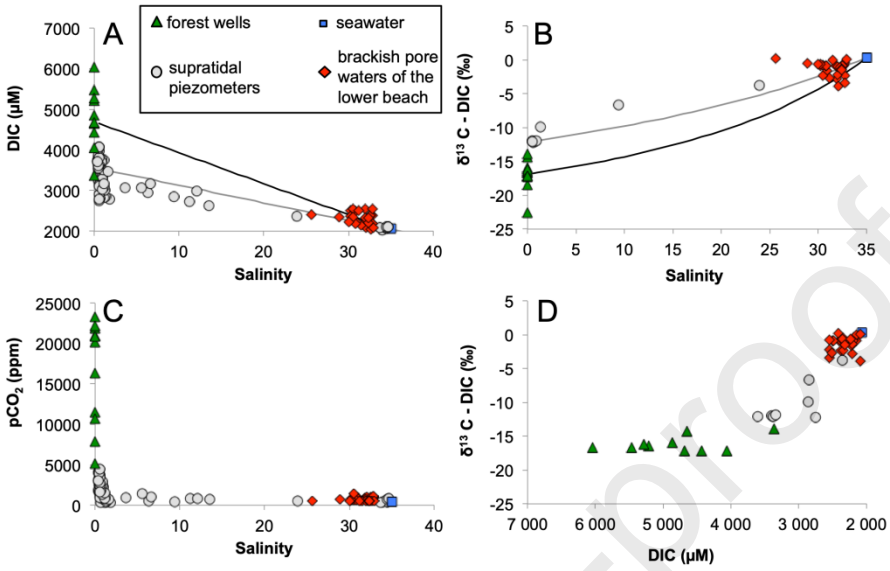

Figure 6: Assessment of the behaviour of DIC along the subterranean estuary of the Truc Vert Beach: (A) DIC concentrations versus practical salinity; (B) δ^{13}C-DIC versus practical salinity; (C) pCO_2 versus practical salinity; (D) δ^{13}C-DIC versus DIC concentrations. The grey lines denote the expected DIC (A) and δ^{13}C-DIC (B) values for conservative mixing between supratidal beach freshwaters and seawater. The black lines denote the expected DIC (A) and δ^{13}C-DIC (B) values for conservative mixing between continental freshwaters (forest wells) and seawater.

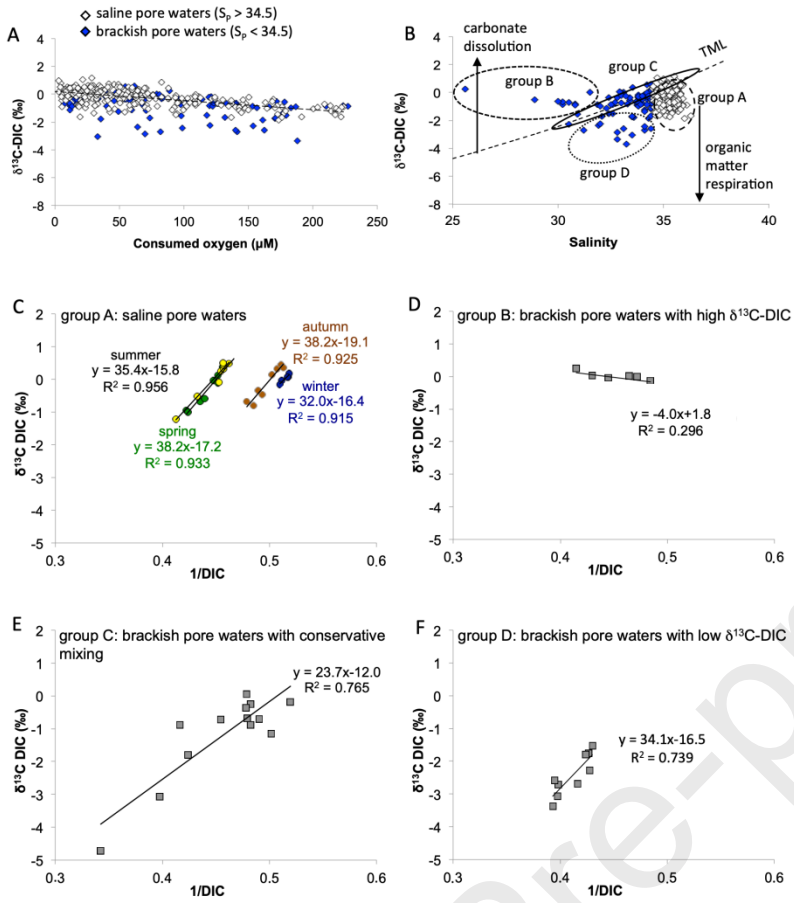

Figure 7: The δ^{13}C-DIC of pore waters from the lower Truc Vert Beach: (A) δ^{13}C-DIC versus consumed oxygen in saline (S_P > 34.5; light grey diamonds) and brackish (S_P < 34.5; dark grey diamonds) water; (B) δ^{13}C-DIC versus practical salinity and definition of four groups of pore waters depending on the mixing behaviour between supratidal beach fresh groundwaters and seawater. TML = theoretical mixing line; (C) Keeling plot of DIC-enriched, saline (S_P > 34.5) pore waters with low δ^{13}C-DIC for each of the four seasons in 2011; (D) Keeling plot of DIC-enriched brackish pore waters characterized by high δ^{13}C-DIC; (E) Keeling plot of brackish pore waters placed close to the theoretical mixing line and little affected by respiration processes (O_2 > 85%); (F) Keeling plot of DIC-enriched brackish pore waters with low δ^{13}C-DIC values and affected by respiration processes (consumed O_2 > 100 µM).